ABSTRACT

ZHANG SHU. Mechanical and Physical Properties of Electrospun Nanofibers (under the direction of Dr. Wendy E. Krause).

The process of electrospinning was utilized to fabricate randomly aigned nylon6 nanofibers and aligned nylon6 nanofibers. Polymer concentration affecting electrospinning was investigated. This parameter was evaluated using degree of crystallinity by differential scanning calorimetry (DSC) as well as visual images produced by scanning electron microscopy (SEM). DSC data demonstrated that more crystals were formed with lower polymer concentrations; SEM images revealed that larger fibers were produced by using parallel electrodes. The mechanical properties of unoriented fibers and aligned fibers were tested on Instron. The result of tensile tests indicated higher Young's modulus and tensile strength of aligned nanofibers than that of unaligned fibers. The SEM images at broken edges of fibers illustrated different broken mechanisms of these two forms of nanofibers. The broken mechanism of aligned nanofibers was further confirmed by crystallinity parameters obtained from DSC and fiber diameter shown from SEM images.

Mechanical and Physical Properties of Electrospun Nanofibers

by
Shu Zhnag

A thesis submitted to the Graduate Faculty of
North Carolina State University
in partial fulfillment of the
requirements for the degree of
Master of Science

Textile Chemistry

Raleigh, North Carolina

August 7, 2009

APPROVED BY:

_____	_____
Wendy E. Krause Committee Chair	Alan E. Tonelli
_____	_____
Russell E. Gorga	Xiangwu Zhang

BIOGRAPHY

SHU ZHANG was born in Jiangxi, China on August 13th, 1984. Initially her parents gave her the name Shu meaning “fairy lady” in Chinese. She had a wonderful and girly childhood with that name. But when she entered elementary school, her parents changed her name to another Shu, which makes her name a complete phrase meaning “open the book”. After that, she became fascinated by knowledge since she realized the special meaning of her name. Shu began her college career at Nanjing University of Technology, where she graduated with a Bachelor of Science degree in Light Chemical Engineering in 2006. While attending Nanjing University of Technology, Shu participated in many activities such as commissary in charge of studies, campus trading management committee and volunteering in the Yong Women’s World Cup of Softball, which strengthened her intelligence, morality and sense of social responsibility. During her undergraduate studies she began to explore the topic of polymers and fibers, which motivated her to continue her education at North Carolina State University and pursue a Master of Science Degree in Textile Chemistry.

ACKNOWLEDGMENTS

I would like to thank GSSP program of North Carolina State University that sponsored my research and study which leads to completion of this thesis. Thanks to my parents for their love, encouragement and support through the most challenging times and throughout all my life. Thank you to all my friends for helping me solving all kinds of technical problems and refilling me with relief and joy when I was exhausted.

I would like to thank my advisor, Dr. Wendy Krause, for her guidance throughout this study. I would also thank Dr. Alan Tonelli, Dr. Russell Gorga and Dr. Xiangwu Zhang for being my committee members and reviewing my research. I would also like to thank Nagarajan Thoppey Muthuraman, Sangeetha Ramaswamy and Rebecca Klossner for their discussion and advice during the experiment setup and design and result analysis. I also thank Logan Harvey for all his work on this research.

TABLE OF CONTENTS

LIST OF TABLES

LIST OF FIGURES

CHAPTER 1

INTRODUCTION TO ELECTROSPINNING

1.1 Electrospinning Overview

Electrospinning technology has been known since twentieth century. Electrospinning is an old but yet immature process which is now used to form nanoscale polymer fibers. With a stroke of good luck the electrical phenomenon was first discovered in 600 B.C. The Greek philosopher, Thales of Miletus, noticed that feathers and other light particles were magically lifted off of the ground when placed near a special material which had been rubbed by cloth. This material just so happened to be amber, the fossilized resin of ancient trees, which forms through a natural polymerization process of the original organic compounds. The Greek word for amber is electron, and thousands of years later the world was changed with the realization of this phenomenon and the term “electricity” was born.

The first discovery of electrical effects on liquids occurred 2200 years after Thales of Miletus had first discovered electricity, and in an incredibly similar manner. In 1600 AD William Gilbert observed that a spherical water droplet was pulled into a conical shape when a charged piece of amber was held above it.

In 1902, Morton received the first US patent for electrospinning of artificial fibers [1]. In the 1930s and 1940s, Formhals claimed a series of patents on the process and apparatus to produce electrospun fibers [2, 3, 4, 5]. In 1914, Zeleny presented one of the earliest studies of

electrified jetting phenomenon [6]. However, the practice and study of the electrospinning technology remained largely dormant until 1970s. Similarly, in electrospinning research, only a few publications appeared in the 1970s and 1980s, notably by Baumgarten and by Larrondo and St. John Manley [7, 8].

In Baumgarten's experiment, a glass capillary was filled with an acrylic polymer solution. A charged wire was inserted into the capillary. There was no feed rate control; once a critical voltage was applied, a fluid jet ejected out from the capillary tip. The effect of humidity on the electrospinning process was studied. High humidity caused the fluid to dry improperly. Baumgerten also estimated the jet speed to be around 280 m/s (near the speed of sound) by using energy balance [7]. He has over estimated the charge on the jet. The actual speed is about 10 m/s.

Not much attention was given to the scientific aspect of electrospinning until Doshi and Reneker reintroduced this technique as a facile way to make submicron fibers. Doshi [9] made an effort to characterize electrospinning process using aqueous polyethylene oxide (PEO) solutions as a model fluid, and provided the following process description: he argued that the electric charges in the form of ions moved in the response of electric field and transferred the momentum to the polymer fluid. The jet carried out the electric charge from polymer reservoir to the collect and thus completed an electric circuit that provides the energy required to drive the flow. A decrease in jet diameter was attributed to stretching of

the jet and solvent evaporation. When the jet diameter became sufficiently small, radial forces due to the electric charge became large enough to overcome the cohesion forces of the fiber, and this caused the jet to splay into many smaller fibers. This jet division occurred many times in rapid successions, and produced a large number of small charged fibers moving toward the collector. The divided jet repelled each other, thereby acquiring lateral velocities and chaotic trajectories. Charged fibers were collected on a ground metallic screen. The observed diameter ranged from 0.05 to 5 μm, and fibers possessed a wide variety of cross-sectional shapes, e.g. coils and beads. This process was generally accepted and adopted in subsequent studies, such as Reneker and Chun [12].

Since then the utilization of electric field to produce nano-sized aerosols and fibers has gained much attention. The number of publications in this area has been increasing exponentially in the past 15 years (see Fig.1).

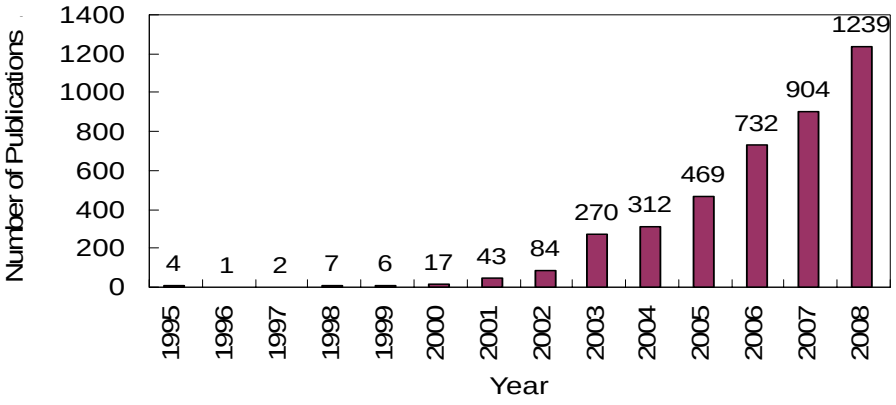

Figure 1.1 The annual number of publications on the topic of electrospinning, as provided by the search engine of SciFinder Scholar. For 2009, there are already 174 before March 12.

1.2 General Experimental Description

For electrospinning to occur one needs a relatively simple set-up. Electrospinning devices come in different size and shapes. The components include a power source capable of forming large electric field (0.5 kV/cm), a grounded counter electrode, a viscous solution, and a means of pumping the liquid. While a solution is forced out of the nozzle, either by gravity or external force, the immediate forces acting upon liquid are gravity, surface tension, and electrical stresses. These forces compete and balance each out to form Taylor cone, and depending on the status of equilibrium the cone will eject nothing, droplets, or a jet of liquid that travels to a grounded collector.

Often in laboratory practice, the applied voltage and the flow rate of the fluid are closely regulated. In a more elaborate electrospinning device, a pumping device is used to deliver the fluid to the capillary. Usually, the fluid is fed through a non-conducting tube to the capillary to prevent unwanted electrical discharge to the pump. A typical voltage generator delivers 10 to 40 kilovolts at around 100 microamperes of direct current (DC).

A typical distance between the nozzle and the collector is 10 centimeters or more. The fiber collector comes in myriad designs. The most basic one is just another metallic disk or plate that is connected to a grounded wire. The more complicated designs may include a coagulating solvent bath or a conveyor belt. There are several ways to control the alignment of the depositing fiber. One way is to use a rotating wheel blade to collect well-aligned

segments of the fiber [10]. One other way is to deposit the fiber across a small air gap between two collectors. Another way is to use a series of charged rings to direct the electrospinning jet onto the collector [11]. Additional methods will be discussed in section1.3.4.2.

1.3 Process Description

The electrospinning process is characterized by four major regions: (1) the Taylor cone region, (2) the steady jet region, (3) the instability region, and (4) the base region. The jet initiates at the bottom of the Taylor cone and then travels as a single jet decreasing in diameter toward the ground electrode. At some point the jet experiences instability from surface charge effects and nearly disappears to the naked eye. At this point the jet experiences what is most commonly referred to as ‘whipping’ instability, where the jet is accelerated, stretched, and dried. The final region as described by Reneker [12] is the collection region. It is here that the jet and instability are stopped and the fibers are collected.

1.3.1 Region 1: The Taylor Cone

The conical formation occurs from a combination of charge repulsion and surface tension mechanisms. Since there is an electric field being applied between the nozzle and a counter electrode an electric stress is induced in the droplet with both normal and tangential components. When the electric field and liquid flow rate are in a precise range the electrical stress will overcome the surface tension of the liquid. When the surface tension is overcome

a Taylor cone forms [13]. The tangential electric field will then accelerate charge carriers in the liquid, which then accelerates the surrounding liquid toward the counter electrode in an attempt to complete the circuit.

The drift velocity of ions in a solution can be calculated by multiplying the electric field by the ion mobility. For example sodium ions have a mobility of 1.5×10^{-7} $m^2/(Vs)$ in water at room temperature and viscosity of 1.002×10^{-3} Pa s, when the applied electric field is around 10^6 V/m [14]. This velocity is can be estimated as on the order of 0.15 m/s for sodium ions in this liquid. This causes the cone to eject either a spray or jet of liquid depending on viscosity of the solution [14]. Due to the high surface charges on the ejected material the droplets or fibers produced remain highly charged until they can be discharged by either a corona of ions or by electrical conduction. This takes a long time for materials with a large dielectric constant. This charge however can be beneficial in the case of enhanced filtration, commonly known as electric filtration. Taylor calculated that the surface tension stress perfectly balances with the electric normal stress to create a cone with apex angle of 98.6^o. His cone is assumed to have no loss of material though by either spraying or spinning, so scaling laws have been derived which predict droplet size and the current as a function of liquid properties and flow rates [15]. Material properties exist which one can use along with scaling laws derived [16] to estimate this conical shape.

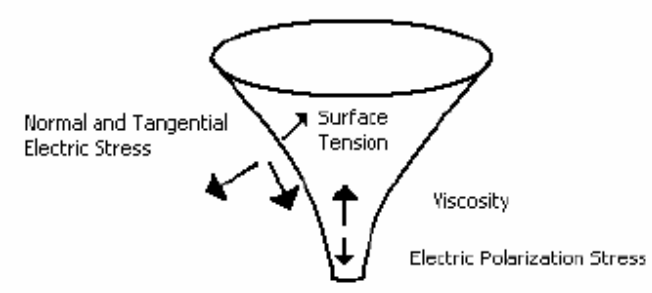

Figure 1.2 Forces in the liquid cone [16].

1.3.2 Region 2: The Jet

The general description of the steady jet is within the realm of electrohydrodynamics. Numerous publications have addressed the behavior of the jet before the onset of the whipping instability[17, 18, 19, 20, 21]. Harthman et al. have devised a scaling law for the diameter and surface charge of a fiber being emitted from the bottom of a Taylor cone. The equations are as follows:

$$d_j = b_{jet} \bullet Q^{a_{jet}} \qquad Equation\ 1$$

$$\sigma = \frac{0.59 I d_{jet}}{4Q} \qquad Equation\ 2$$

d_{jet} = jet diameter (m)

b_{jet}, a_{jet} = scaling constants

a_{jet} = 0.71

Q = flow rate (m^3/s)

I = current through jet (A)

σ = surface charge on jet

These equations are not applicable for the instabilities which result in nanometer diameter fibers. Without proper control of operating conditions or fluid properties fibers can form with beads distributed throughout, or if the evaporation of solvent does not occur, the fibers will collect in a puddle on the collector.

Fridrikh et al. [22] predict that a terminal fiber diameter exists for electrospinning of polymers. The terminal jet diameter is reached when there is a final balance of all stretching forces with the surface tension. The outcome of the balancing of all forces results in the Equation 3.

$$h_t = (\gamma \bar{\varepsilon} \frac{Q^2}{I^2} \frac{2}{\pi (2 \ln \chi - 3)})^{1/3} \qquad Equation\ 3$$

H_t = terminal fiber diameter

$\bar{\varepsilon}$ = permittivity of surrounding fluid

Q = flow rate

I = current

χ = radius of whipping curvature / fiber diameter – a dimensionless wavelength of the instability responsible for the normal displacements

The terminal jet diameter is thus dependant directly on the flow rate, electric current, and surface tension of the fluid. This equation also suggests that there is a cica six fold variation of fiber diameter with flow rate. Their equation also predicted the fiber diameter successfully

for poly-caprolactone (PCL) when a scaling constant for the polymer concentration is introduced. It is also predicts the final diameter for PEO solutions at 10% accuracy and PAN fiber at 20% accuracy. The reason that the model predicts the diameter for PEO and PAN successfully without having to incorporate a correction factor for polymer concentration is most likely due to the specific charge carrier inherent to the system. The conductivity of PCL was < 1μS/cm, and the charge carrier was the solvent.

For the PEO and PAN systems the primary charge carrier is the polymer [23], and the solvents were water and N,N-dimethyl formamide, which are not very volatile. When a volatile solvent is the main charge carrier, charges are lost as the solvent evaporates. This gives rise to a lower surface charge density than theoretically calculated, resulting in a larger diameter fiber.

This prediction is under the condition that no other fiber thinning mechanisms occur. Splaying also has been observed [24]. Fibers produced from splaying events are typically 1/3 the diameter of the fibers of the primary population. By splaying the electrospun fiber can further reduce its surface charge density, thereby making it more stable.

For fiber formation to occur it is necessary to have a solvent with a high vapor pressure, such as an alcohol. System using water as a solvent have been shown to work as well, yet if the vapor pressure is not high enough then fibers do not form. This proves challenging when dealing with ceramic precursor alkoxides as some tend to react when in combination with

certain polymers and alcohols. Trials using di-ethylene glycol monoethyl-ether, which has a boiling point of about 200^{o}C, rendered no useful fiber due to the lack of evaporation of solvent [24]. A puddle of solution resulted. An increased working distance between the capillary and collector may help.

To fabricate a uniform fiber, surface tension and surface charge act in competition, while viscosity plays a major role as well. Surface tension tries to minimize specific surface area, by changing jets into spheres. On the other hand an excess electrical charge tries to increase the surface area, which would favor making thinner jets. All the while the viscosity of polymers resists rapid changes in shape [25].

As the viscosity of a solution is increased, bead size increases, and the shape of the beads becomes more spindle shaped than spherical. As net charge density increases the beads become smaller and more football shaped as well. Decreasing surface tension makes the beads disappear. Therefore for a thin, stable jet, it is important to look for a balance of viscosity charge density, and surface tension.

Excellent SEM images of these relationships are demonstrated in reference [12] and the reader is referred to that publication. The investigation researched effects of viscosity, ionic conductivity, and surface charge density. Reneker used a corona discharge to neutralize charge on the fiber as it was being produced. As the fibers were neutralized charge on the

fiber as it was being produced. As the fibers were neutralized more bead formation occurred, confirming the analysis of surface charge density on stable fiber formation [26].

1.3.3 Region 3: The Instability Region

As the jet is ejected from the bottom of the Taylor cone, it will remain stable for a certain distance which is specific to each solution and electrical configuration e.g., a point to plate or parallel plate setup. Intensive electric relationships occur throughout the jet due to the number of fluid, equipment, and operating variables that can alter any electrospinning operation. No theory exists that can take into account all variables and describe the process with quantitative accuracy. However, Rutledge et al. have created the most in-depth theory of the jet and instability regions to date [22, 25-28]. Table 1.1 illustrates the variables which should be taken into consideration.

Originally, the jet was believed to splay into multiple jets orders of magnitude smaller than the initiating jet [12]. High speed photography has disproved this theory and demonstrates that in reality the jet whips so fast it looks like multiple jets but in reality is one jet [26]. Splaying events do occur, though they do not decrease the jet diameter by orders of magnitude. As the jet travels toward the collector, the surface charge density changes along with the diameter of the jet, and results in various instabilities.

Table 1.1 Factors affecting electrospinning

Fluid Properties	Operating Parameters	Process Variables
*Viscosity	*Flow Rate	Jet Radius
*Conductivity (K)	*Applied Electric Field (V)	Axial Velocity
Dielectric constant (ε)	Jet Current (I)	Charge Distribution
Surface tension (γ)	Distance (d)	Centerline Displacement

* most important variables

The high-speed photographs suggest that each fluid element does not travel along the spiraling path but rather travels radically outward from the center and downward to the collector, like water streaming away from a water sprinkler. 10 successive images were taken as 2-D projections of the jet, with a 0.001856 second interval time between each frame. The whipping instability of this jet has been observed to have a well defined period, wavelength, and amplitude. The amplitude is growing exponentially as the jet travelling further away from the needle.

Three main instabilities exist (Figure 1.3A) and each can be thought of as acting independently and competing for stability. Much like the various phases of a metal competing for thermodynamic stability, these areas of instability compete for stability and an operating diagram, much like a phase diagram, can be created for individual polymer solvent system [28]. These instabilities vary and increase with distance, electric field, and fiber

diameter at different rates depending on the fluid parameters and operating conditions. Each instability grows at different rate. Whichever instability is largest at a particular time is the stable instability. To attain a desired instability these calculations can be carried out or one can make 'real time' changes and observations to the operating parameters to obtain desired results.

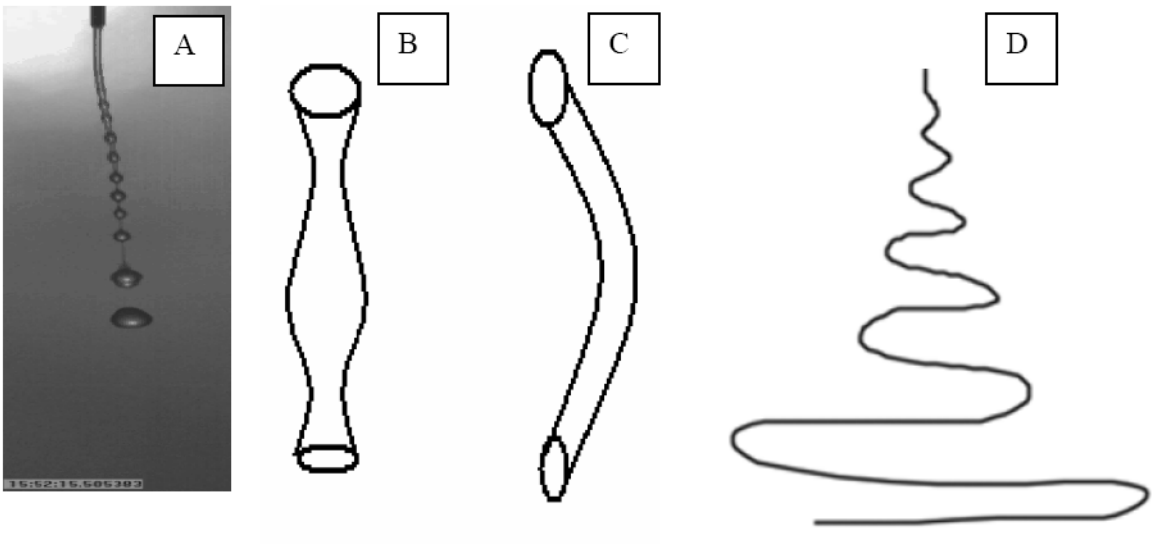

Figure 1.3 Instabilities in the jet (A) Rayleigh instability (B) axisymmetric conducting instability (C) bending instability which results in whipping (D) whipping instability [28].

The first instability encountered is the Rayleigh instability at low electric fields, and is most dependent on the surface tension of the material. Two other instabilities arise with an application of higher electric fields and are dependant on the conductivity of the solution. The model referenced realizes that the instabilities occur with wavelengths that are quite

longer than the jet radius. This allows the jet to be modeled as a slender object of great length which simplifies the equations used to model a Newtonian fluid jet.

1.3.3.1 Rayleigh Instability

The first mode of instability for a droplet under an electric field is an increase in dripping corresponding to small droplets being emitted from the capillary (Figure 1.3A). This instability is axisymmetric and suppressed when the applied electric field, E_∞, and surface charge density σ exceed a limit given by Equation 4 [29].

$$(\varepsilon - \bar{\varepsilon})E_\infty^2 + \frac{4\pi^2\sigma^2}{\bar{\varepsilon}} = \frac{2\pi\gamma}{h} \qquad \textit{Equation 4}$$

- γ = surface tension
- ε($\bar{\varepsilon}$) = dielectric constant inside and outside the jet, and (ε/$\bar{\varepsilon}$) >>1
- E_∞ = External electric field
- h = fiber diameter
- σ = surface charge density

The Rayleigh instability is generally referred to as a non-conducting mode instability because the conductivity of the medium does not play an important role. It is the surface tension which is important.

1.3.3.2 Axisymmetric Conducting Mode

The next mode of instability encountered is dependent on the finite, nonzero conductivity of the fluid. Axisymmetric conducting instabilities can be visualized as a direct competition between the surface charges with the surface tension of the fiber, while the fiber is moving (Figure 1.3B). Although the literature has not attributed bead formation to axisymmetric instability, it does seem similar. The fiber tends to thin and bulge at a specific frequency which is dependent on the surface charge. According to the literature an excess surface charge exists at the bulges and a smaller surface charge density exits at the thin areas of the fiber. The theory can be found in these references [26, 27].

1.3.3.3 Whipping Conducting Mode

The whipping instability is non-axisymmetric and accounts for the small diameters of fibers which can be produced via electrospinnin. This instability is a result of small bends in the initial uniformly charged straight fiber formation. As the fiber bends, the surface charges around the circumference of the jet are no longer uniform and a dipolar moment P(z) is induced perpendicular to the jet. These dipoles initiate a localized torque, in response to each other and the applied electric field. This torque bends the jet (Figure 1.3C). The bends amplify as the jet moves further downstream thus becoming the whipping instability that causes the decreased diameter of the fibers (Figure 1.3D). The jet is further decreased in diameter (up to 3 orders of magnitude) by solvent evaporation [30].

The modeling for the whipping mode is intensive and can be left to the interested reader to read in its entirety in the publications from Rutledge's group.

The decrease in diameter due to the whipping instability is assumed to be a result of the increased path length that the jet travels as a result of the complex relationship between surface tension, viscosity and acceleration of jets surface charges and internal charges by the external electric field.

1.3.3.4 Competition of the Modes

Each of the modes of instability increases according to the variables which accounts for their respective instability with a so-called amplification factor Γ (E_∞, Q), where E_∞ and Q are the external electric field and the flow rate respectively [25].

A diagram much like a phase diagram can represent the competition of various growth rates as they are dependent upon applied electrified field and flow rate. From the growth rate equation, $d\ln A/dt=\omega(h,E,\sigma)$ where A(t) equals the amplitude of a perturbation at time t. By making the approximation that $dA/dt \sim UdA/dz$, where $U=Q/\pi h^2$, the flow rate divided by the area of that section, an amplification factor can be obtained at a distance d, downstream.

$$\Gamma(E_\infty, Q) = \ln\left[A(d)/A(0)\right] = \int_0^d \frac{\omega(h,E,\sigma)\pi h^2}{Q} \qquad \textit{Equation 5}$$

- E_∞ = external electric field

- E = local electric field
- Q = volumetric flow rate
- σ = surface charge density
- h = radius of jet

This calculation predicts that the whipping instability will predominate at high field strength and flow rate, while the axisymmetric instability and Rayleigh instability predominate at lower flow rates and electric fields.

1.3.4 Region 4: The Base

The base is the final region of the electrospinning apparatus. It must consist of an electrode of opposite charge for the fibers to be accelerated to. Different electrodes and electrodes orientation have been utilized by numerous researchers such as a flat piece of metal, a screen, or even a rotating drum [31]. The typical electrode used in this study is aluminum foil, due to its inexpensive price, availability, and ease of changing for the analysis of many samples. The foil is connected to a ground electrode to provide a path for the current to travel. It is of utter importance to study the current passing through the sample so that the surface charge densities can be calculated. This can be measured by connecting a resistor in line with the ground, and measuring the voltage drop across the resistor with a multimeter.

1.3.4.1 Flat Collector

This is the most widely used method of fiber collection. The collector can be either a solid metal, foil, or screen. Other materials can also be placed in between the capillary and the collector. Donaldson Inc. has successfully placed cellulose fibers between the capillary and collector to coat them for filtration purposes [32].

1.3.4.2 Aligned Nanofibers

(A) Rotating drum

In the approach of Katta et al. [33], the grounded platform for collecting the nanofibers is a copper wire-framed drum. The drum has two circular nonconducting Plexiglas disks. The two disks are mounted on a rod and spaced apart with PVC pipe. The copper wire is stretched between the slots cut into the edges of the disks shown in Figure 1.5. The copper wire is grounded. The polymer solution was forced through a stainless steel needle using a syringe pump at a constant rate. The drum was located fifteen centimeters below the needle.

Individual nanofibers cannot be seen with the naked eye, but after 5 min of spinning, a nanofiber sheet oriented perpendicular to the symmetry axis of the wire drum was observable. Many of the nanofibers collect directly on the copper wire closest to the needle. As the drum slowly rotates, the next copper wire attracts the nanofibers and the nanofibers stretch perpendicular to the copper wires to span the gap between the wires.

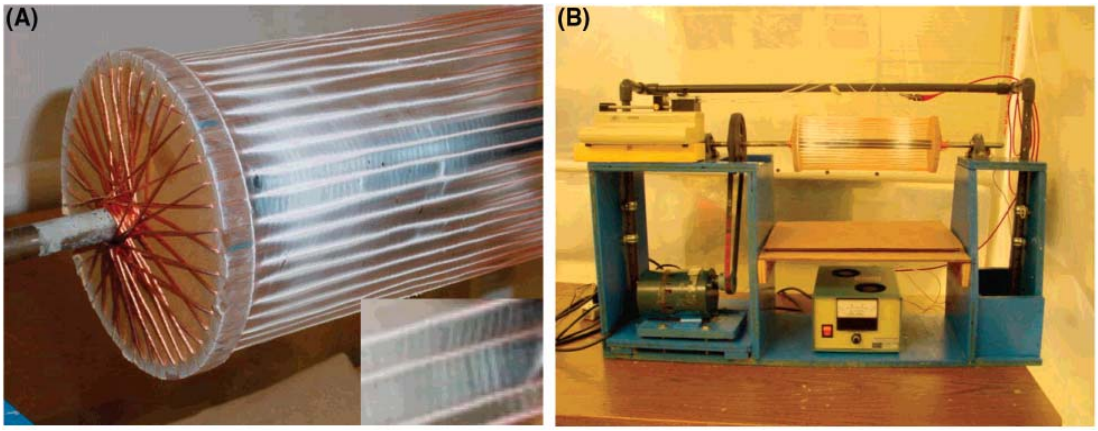

Figure 1.4 (A) Plexiglas disk with copper wires. Electrospun nylon 6 nanofibers are collected on the copper wires. The nanofiber mat shows stratified layering in the magnified image. (B) Apparatus for rotating the copper wire drum during electrospinning [33].

Alignment of the nanofibers is driven by electrostatic interactions allowing the charged nanofibers to stretch and span across the gap between the wires and to form axially aligned arrays over large areas. The charged nanofiber experiences two sets of electrostatic forces: the first set originates from the applied electric field and the second one between an incoming section of charged fiber and charges on the surfaces of fibers attached to the wires. The first electrostatic force is in the same direction as the applied electric field, hence the nanofibers move to the vicinity of the copper wires. Because of the rotation of the drum a given wire is closest to the needle for a short period of time. As the rotation continues the next wire rotates closer to the needle. The electrospinning fibers follow the electric field attraction of the next wire and thus the fibers move from one wire to the next. Due to the second set of electrostatic

forces the fibers stretch across the shortest distance in the gap between the wires and thus cause the fibers to align.

The limitation of this study is the loss of alignment with thicker mats. After electorspinning for a certain time, fibers started entangling and being disturbed, but it is still not understood according to this study.

(B) Parallel electrodes

There has already been several groups produced well-aligned nanofibers by using two grounded parallel electrode, such as aluminum strips with a 1cm gap used in Yi Xin's group [34] and the metal frame in Dersch's group [35] et al.. The observed orientation is believed to be due to the polymer jet jumping back and forth from one side of the frame to the other, apparently because of electrostatic charging effects. This apparatus used in this method is very simple. The same as the rotating drum method, it works by modifying the collectors. The drawbacks of both these two methods are that a). they can only produce aligned fiber in a small area, and b) fibers fabricated by this method cannot be conveniently transferred to different types of substrates.

(C) Dual vertical wire technique

The dual vertical wire technique used in Surawut's study [36] is a modification to the parallel electrodes technique, comprised two stainless steel wires, used as the secondary target, and

the grounded aluminum foil, used as the primary target. The two stainless steel wires are mounted vertically in parallel to each other along a center line between the tip of the needle and the grounded aluminum foil. Both the needle and the foil were tilted about 45° from a vertical baseline.

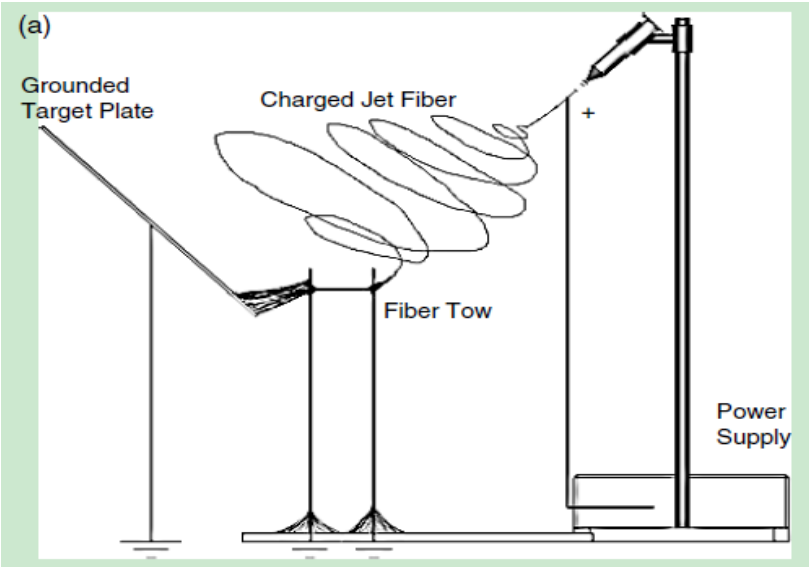

Figure 1.5 Side view of the schematic setup of the dual vertical wire technique [36].

The authors also tried to use the secondary electrodes alone, but much smaller amount of aligned fibers was obtained. This was because the majority of the fibers would instead deposit randomly around the first wire electrode. Based on this observation, both the primary and secondary electrodes were essential elements for getting well-aligned fibers for the present setup. The mechanism for the depositing fibers to stretch across the wire electrodes is similar to the parallel electrodes described previously. By this setup, both aligned fibers

(between the parallel vertical wires) and a randomly-aligned fiber mat (on the aluminum foil) could be achieved.

(D) Using a insulating tube on the collector

Ying Yang et al. produced a large area of oriented fibers by putting an insulating tube on the target for a long time [37]. The modified electrical field made the jet bend around the tube, so the oriented fibers could be received with a suitable tube.

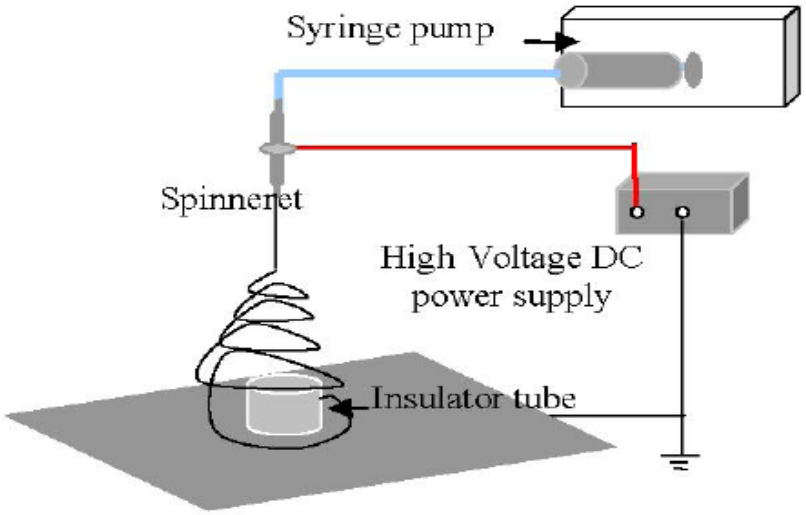

Figure 1.6 The setup schematic illustration of insulating tube on a collector [37].

Based on different height and diameter of the tube, there were three kinds of collection of aligned fibers formed: (a) only a round mat within the tube area, (b) a round belt outside the tube and a round mat within the tube area, and (c) only a ring belt outside the tube area.

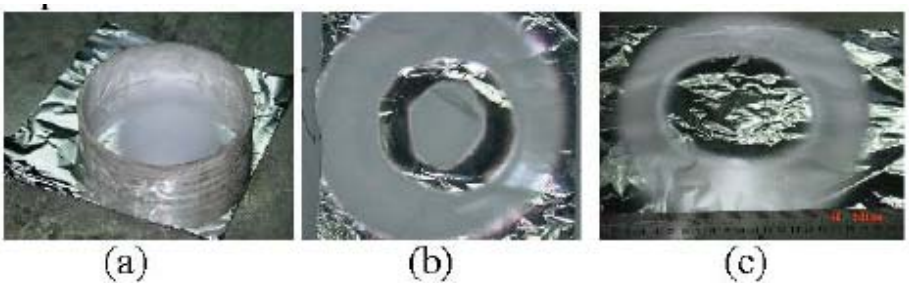

Figure 1.7 Three kinds of collection of fibers obtained by insulating tube method [37].

However, since there is only one electrode as the target, the repelling force is not large enough on the tube to keep the jet falling around the tube all the time. In this case, the jet is not coaxial with the tube and results in disordered fibers.

(E) Biased AC electrospinning

Biased AC electrospinning is a relatively new method used by Soumayajit Sarkar et al. [38]. It employs a combination of DC and AC potentials. This study aimed at minimizing the inherent instability of the fiber itself, comparing to all those four techniques discussed above relying on minimizing the fiber instability by applying external forces on the fibers during electrpspinning. By introducing a DC biased AC potential instead of either a pure AC or DC potential, the authors believe alternating positively and negatively charged regions in the fiber could result in a decrease in electrostatic repulsion and increase in fiber stability.

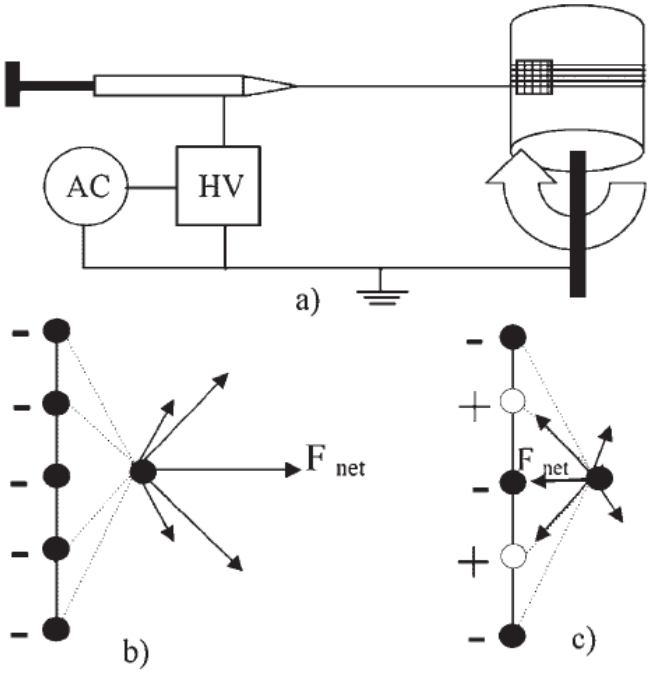

Figure 1.8 (a) Schematic diagram of the electrospinning apparatus. Force balance on a displaced segment of an electrically charged fiber in (b) DC electrospinning and (c) AC electrospinning [38].

However, apparently the authors considered fiber stability as identical to fiber alignment. Stability can improve electrospun fiber quality, but it is not necessary the reason for the fibers to be aligned. Furthermore, the paper mentioned the rotating drum used in their setup could significantly impact fiber morphology. And there is no further information to eliminate the contribution of rotating drum to formation of aligned fibers. Therefore, the method used in this research is not convincible enough to act as a new technique to produce well-aligned fibers. Instead, it provides a way to improve resultant fiber qualities by stabilizing the fiber itself.

(F) Magnetic electrospinning

Dayong Yang et al. employed the magnetic electrospinning (MES) technique to fabricate well-aligned nanofiber arrays and multilayer grids. MES simply requires adding two magnets to a conventional setup[39].

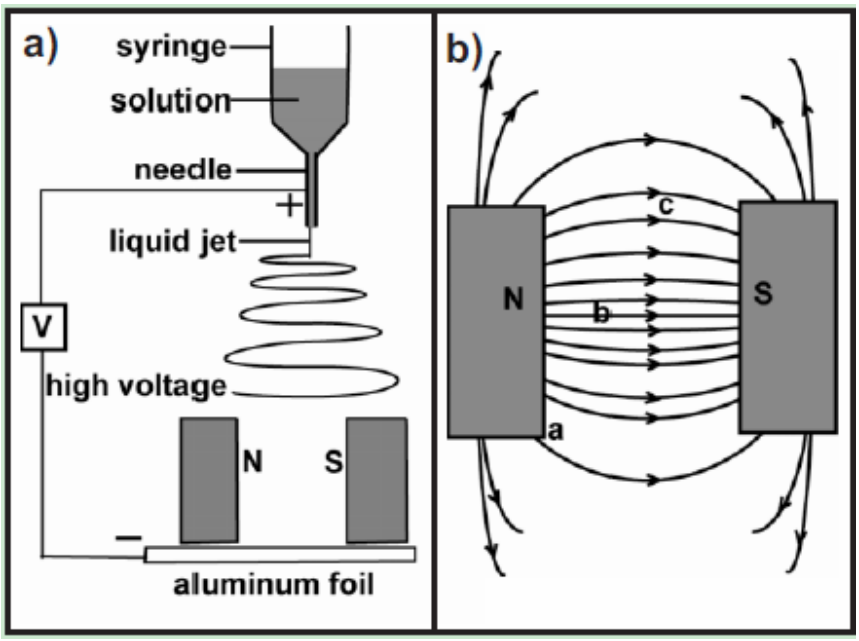

Figure 1.9 a) Illustration of the apparatus for magnetic electrospinning (MES) to generate aligned fibers. The key component of the system is a magnetic field generated by two parallel-positioned permanent magnets. b) Calculated magnetic field strength vectors in the region between the two magnets (top view). The arrows denote the direction of the magnetic field lines [39].

In MES, the polymer solution is magnetized by the addition of a small amount of magnetic nanoparticles. The magnetic field stretches the fibers across the gap to form a parallel array

as they land on the magnets. When the fibers fall down, the segments of the fibers close to the magnets are attracted to the surface of the magnets, finally the fibers land on the two magnets and suspend over the gap.

The MES method is fundamentally different from all previously discussed methods in preparing aligned fibers, because the driving force is magnetic field in MES while electrostatic interaction plays the role as driving force in the other methods. MES has several advantages: a) the magnetic field can be manipulated accurately; b) the resultant nanofibers can be transferred onto any substrate with full retention; and c) the area of the aligned fibers is large compared to other techniques.

1.4 Potential Applications

1.4.1 Tissue Scaffoldings

One of the most promising potential applications is tissue scaffolding. The nonwoven electrospun mat has a high surface area and a high porosity. It contains empty space between the fibers that is about the size of cells. The nonwoven mat has the approximated architectures that can mimic the *in vivo* condition for cells. The mechanical property, the topographical layout, and the surface chemistry in the nonwoven mat may have a direct effect on cellular proliferation and migration [40]. The electrospun mat may provide mechanically stable scaffolding, in which cells can proliferate. Then, the cells synthesize

their own extracellular matrix to form a functional tissue while the electrospun mat degrades away.

One of the earliest works was a study on the proliferation of smooth muscle cells in an electrospun collagen mat [41]. Type I and type II collagens were chosen due to their relative non-immunogenic nature and mechanical stability. The collagens were first dissolved in hexafluoropropanol. Then the solution was electrospun into a fibrous collagen mat. The electrospun collagen fiber mimics the molecular and structural properties of native collagen. The electrospinning process induced the collagen molecules to form α-helical domains, forming a periodic banding pattern in the fiber. The researchers claimed that these banding patterns promote structural integrity and biological activity, which can provide an *in vivo*-like environment for cells to grow. The size of the electrospun collagen fiber is about 100 nm in diameter, very comparable to the size of collagen fibrils found in native tissue. Aortic smooth muscle cells were seeded into these electrospun collagen mats. When the cellular growth was examined, it was found that the cells were able to infiltrate and to proliferate in the mat.

In addition to naturally occurring materials, researchers also have tried synthetic materials. Li et al. presented one of the first works on the feasibility of using a synthetic electrospun mat for cell culture [42]. They selected a synthetic polymer called poly(D,L-lactide-co-glycolide), which is biodegradable and has been used in clinical applications. The mechanical properties

of the electrospun mat are comparable to those of human tissue. The cells were able to proliferate to confluency in 7 days.

Since 2000, researchers have tried to electrospin different materials into viable tissue scaffoldings. In the same period, researchers have tried to seed different types of cells in trying to develop functioning tissue, such as skin, heart valves, nerves, blood vessels, and cartilages [43-49]. A fully functioning human tissue generated from an electrospun mat has yet to be developed. It has been demonstrated, however, that the electrospun fiber mat is a promising avenue for tissue regeneration in humans.

1.4.2 Templates for Inorganic Fiber

Another potential application of electrospinning is to make inorganic nanofibers. Spinning inorganic materials into nano-sized fibers is difficult. Electrospun polymeric nanofiber mats can provide sturdy templates to create these hard-to-spin inorganic fibers. One method is to coat the electrospun mat with organic materials by chemical disposition. Caruso et al. demonstrated the feasibility of this method by producing a mat of titanium dioxide nanofibers that are hollow [50]. A solution of poly(*L*-lactide) was electrospun into fibrous mat. Then the mat was dipped into a sol-gel of a titanium salt. Once the mat was coated, thermal treatment burned off the poly(*L*-lactide), leaving behind a nonwoven mat of a hollow titanium dioxide fibers. The hollow fiber was about 1 micron in diameter with a wall thickness of 100 nm. The hollow structure creates a large surface area per volume that can

enhance the process efficiency in applications such as catalysis and diffusion. Several other types of inorganic fibers, such as rare-earth compounds and metallic oxides, have been produced using this coating method [51,52].

Instead of coating the fiber mat after electrospinning, blending inorganic materials into a polymer before electrospinning is also possible. Shao et al. blended silica gel with poly(vinyl alcohol) and electrospun this mixture into a fiber mat [53]. Thermal treatment burned off the polymer, forming a silica fiber mat. The silica fiber is not hollow in this case. However, it is quite porous, which generates a large surface area. Other researchers have also used this method to obtain other inorganic fibers [30,54].

Fine carbon fiber can also be obtained by pyrolysis of an electrospun polymer fiber [55,56]. First, polyacrylonitrile was electrospun into fine fiber about 100-200 nm in diameter. Then heat treatment and pyrolsis followed. The polyacrylonitrile fiber does not burn off, but does pyrolyze into carbon fiber.

1.4.3 Functional Fiber

Another application is to make composite nanofibers. It is easy to dope the polymer solutions with various fine particles before elecrospinning. Different kinds of particles have been used to produce fibers with desirable characteristics. Fong et al. premixed exfoliated montmorillonite clay particles with a nylon solution before electrospinning [24]. The

resulting clay-nylon composite fiber had well-aligned clay particles along it axis. Wang et al. doped the spin solution with superparamagenetic iron particles [49]. This electrospun fiber mat can actuate in the presence of a magnetic field. Hou et al., doped a polyacrylonitrile solution with carbon nanotubes [57]. It was observed that the carbon nanotube were parallel and oriented along the fiber axis. The mechanical properties of the fiber mat improved significantly with the inclusion of carbon nanotubes.

In one application, Ma et al. exploited the surface feature of the electrospun mat to create a superhydrophobic nonwoven fabric [58]. A solution of poly(caprolactone) was electrospun into a fibrous mat. Then the mat was coated with a thin layer of a hydrophobic chemical using initiated chemical vapor deposition process. The combination of mat's high surface roughness and the chemical treatment creates a superhydrophobic surface that has a contact angle of 175°.

In another application, Wang et al. produced a highly sensitive optical sensor using electrospinning [59]. The electrospun mat was doped with a fluorescent sensor to detect heavy metal ions. This electrospun mat sensor has a higher sensitivity than a film sensor due to the high surface area-to-volume ratio of the mat.

Kenawy et al. demonstrated the feasibility of using electrospun mats as drug release agent [60]. A drug was blended into a solution of polymers before electrospinning. They manipulated the chemical composition of the mat to generate different release profiles.

CHAPTER 2

EXPERIMENTAL AND METHODOLOGY

2.1 Hardware Set-up

2.1.1 Basic Hardware Set-up

Many electrospinning setups exist. These can consist of a variety of collectors such as a wire mesh, rotating drum, or a material placed in between the nozzle and collector. The orientation of the nozzle can also be varied. It can have a horizontal point to plate setup, vertical parallel plate setup, or angled capillary configuration. The set-up for unaligned fibers used in this investigation is a horizontal point to plate configuration with a solid collector illustrated in Figure 2.1. The collector plate was made of a plastic round plate with aluminum foil covering it which provides a quick and removable method for obtaining multiple samples.

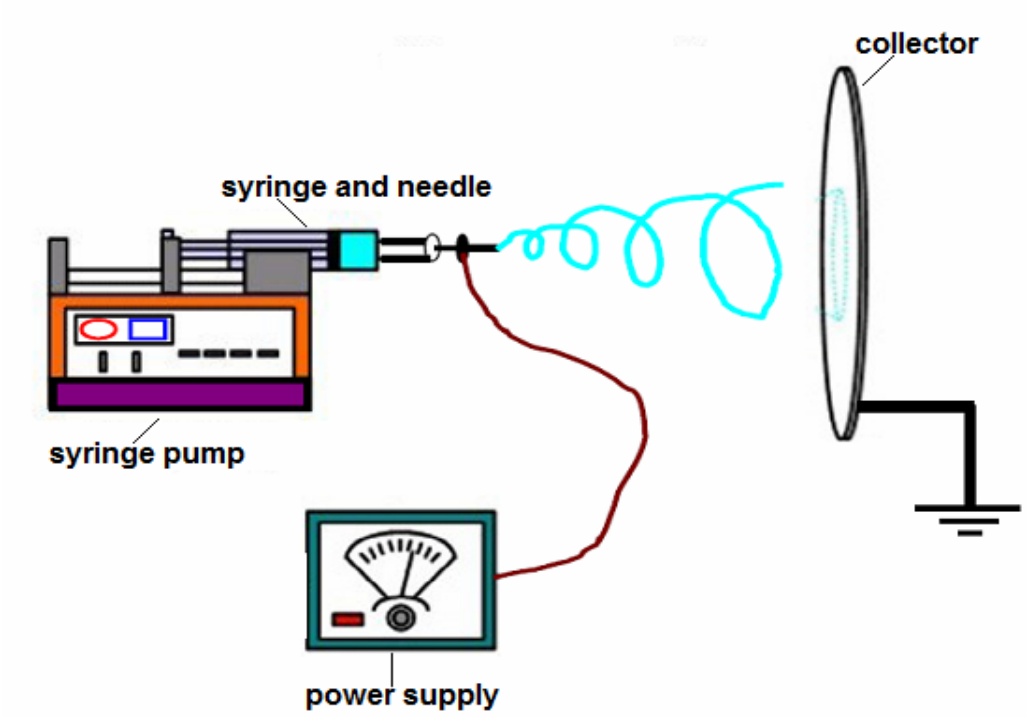

Figure 2.1 Schematic diagram of eletrospinning set-up

The setup consists of a 10 mL medical grade syringe obtained from BD Inc., a 20 gauge needle obtained from Sigma-Aldrich Co., a NE-1000 programmable syringe pump obtained from New Era Pump Systems Inc., and a FC Series 120 Watt Regulated High Voltage DC Power Supply obtained from Glassman High Voltage Inc.

2.1.2 Aligned Experiments

In this study, a straightforward method was used to align electrospun nanofibers. Two grounded strips of parallel electrodes were used (see Figure 2.2).

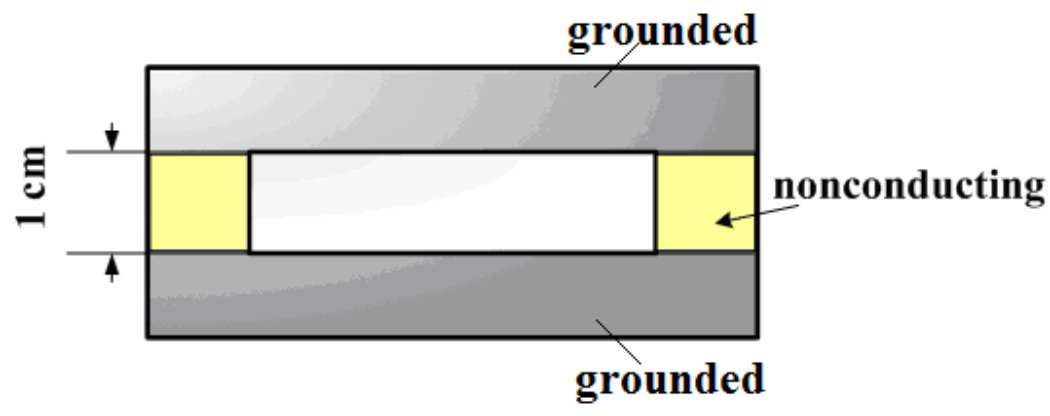

Figure 2.2 Parallel electrodes used to produce aligned fibers in this study

The parallel electrodes were made by a hard paperboard with a rectangular air gap at the center and wrapped with aluminum foil. The concentrations of nylon 6 solution were varied from 10 wt% to 20 wt% to achieve the alignment. During the spinning process, the fibers started to jump back and forth from one grounded side of the frame to the other causing the fibers in the gap to be aligned, as shown in Figure 2.3.

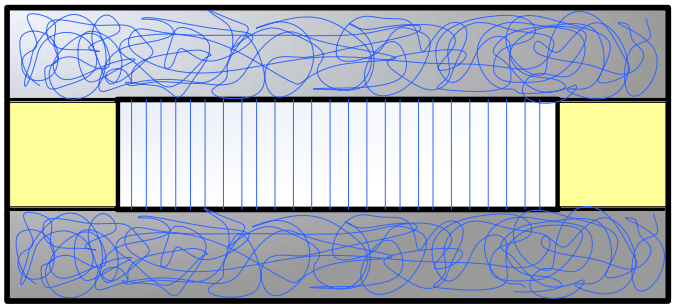

Figure 2.3 Electrodes deposited with fibers.

2.2 Materials

Various concentrations of nylon 6 solution were used with a deionized water and 90% formic acid solvent system. The solution was heated and stirred until a homogeneous solution was formed and electrospinning was attempted and the results were analyzed.

The materials used in the preparation of the various solutions include: a solvent system of formic acid (90%) and deionized water; while the solute is nylon 6. The nylon 6 used in this study is from Sigma-Aldrich Co. and it has molecular weight of 60,000 g/mol. All reagents and polymers were used as received.

2.3 Methods

Various concentrations of nylon 6 were used. After the solvent and the solute were added, the complete solution was stirred on a magnetic stir plate for a period of 24 to 72 hours until the solution was homogeneous. The solutions were then stored in a sealed container at room temperature. The polymer concentrations which produced fibers when electrospun are 15 wt% and 20 wt%.

Electrospinning of the solutions occurred at room temperature. The fully dissolved solutions were drawn into the syringe and a 20 gauge needle was attached. All air is manually removed from the needle by pushing the polymer solution through the syringe until it emerges at the end of the needle. The syringe is then secured in the syringe pump and the flow rate on the

pump is set between 10 and 15 μL/min.

The high voltage supply is connected to the end of the needle farthest away from the syringe pump to prevent interference with the pump from the electric field. An alligator clamp attached to a wire with a plug that fits precisely into a grounded electrical socket was attached to the collector plate to ground the plate. The high voltage supply is then powered on and when a droplet of polymer solution appears at the end of the needle the voltage is turned up to 15 kV.

Typical operating parameters used in this study are flow rates of 10 and 15 μL/min, voltages at 15 kV, and needle tip to collector distance of 15 cm. The parameters were used based on the results of Gorga's research [62].

2.4 Characterization

Electrospun samples were characterized through the polymer crystallinity properties of electrospun fibers by differential scanning calorimetry (DSC), which could have dramatic effect on the mechanical properties of electrospun nanofibers. The information about fiber diameter, diameter distribution and fiber alignment was obtained from scanning electron microscopy (SEM). The thickness of fibrous mats was measured by the thickness tester. The tensile tests were measured to characterize the mechanical properties of produced fibrous mats. Also two kinds of software were employed in image analysis.

2.4.1 Differential Scanning Calorimetry (DSC)

The degree of crystallinity in a polymer is a very important microstructure property to assess because it has an important impact on mechanical property of single fibers. DSC measurements were carried on a PerkinElmer Diamond DSC with a sealed empty pan as the reference and under a nitrogen atmosphere. Samples of about 3 mg were sealed in aluminum pans. The test was performed as follows: the samples were heated to 250 °C at a heating rate of 20°C/min.

By the heat flow curves during this time period, the most important parameter ΔH can be obtained. ΔH is a quantity proportional to the heat to melt the given sample. As all the measurements were done under identical stetting of the instrument, the variation of ΔH can be taken to represent the variations of crystallinity in these samples. It is calculated by the change in enthalpy normalized by sample mass. Also some other useful parameters can be obtained to describe the melting behavior of polymers. Figure 2.4 is a typical DSC curve from one of the samples in this study. T_m is the peak temperature of melting, at which the value of he heat flow is maximum. A is the area of the normalized heat absorption peak.

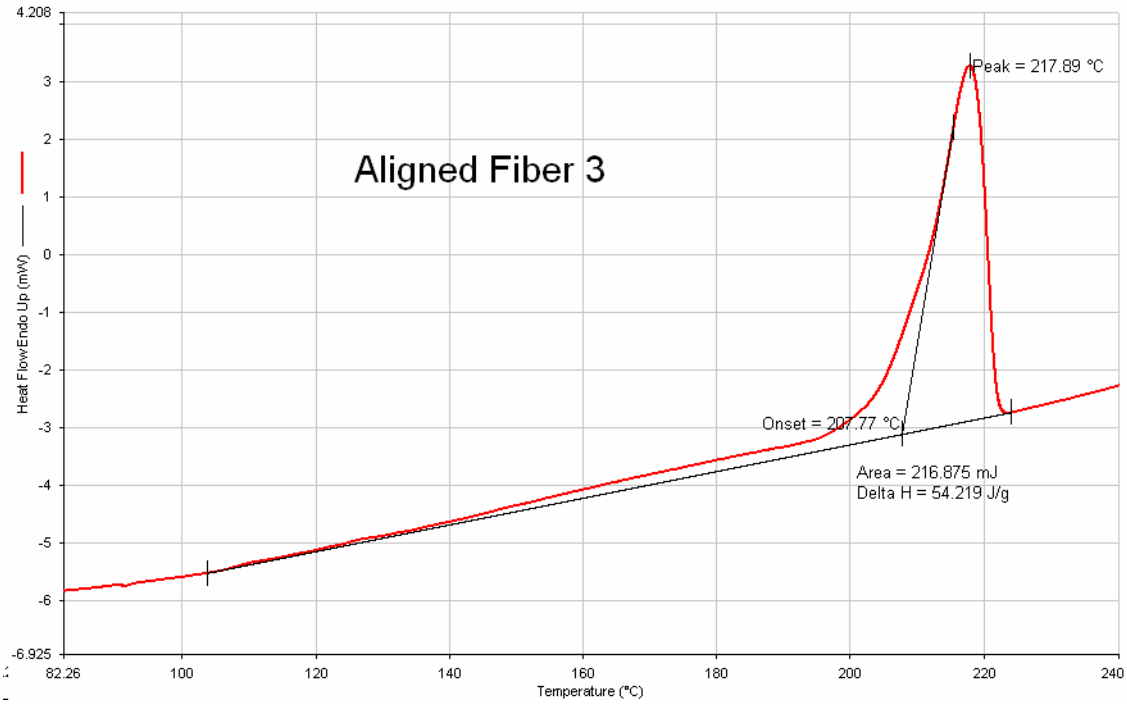

Figure 2.4 DSC curve of aligned fiber electrospun from a 20 wt% of nylon 6 solution, with 15 µl/min feed rate, 15 cm tip-to-collector distance and 15 kV voltage.

The crystallinity of samples was calculated by the formula listed below. The heat fusion of 100% crystalline nylon 6 was taken as 190 J/g.

$$\text{crystallinity} = \frac{\Delta H}{190\ \text{J/g}} \times 100\% \qquad \textit{Equation 6}$$

2.4.2 Scanning Electron Microscopy

The information provided from the SEM images includes fiber diameter, diameter distribution and fiber consistency. This information will be evaluated when determining the

effect of electrospun fiber morphology on breaking fibers.

From the collection material (aluminum foil) samples of approximately 1 cm by 1 cm were cut. The samples were then coated with a layer of gold approximately 100 Å thick using a gold-sputter machine to reduce charge interruptions. Samples were observed by two SEMs: JEOL 6400F Field Emission SEM and FEI Phenom. After samples were mounted on the SEM, they were then focused, and viewed at magnifications between 5,000 – 50,000 times their original sizes. For each piece of electrospun fibrous mat, samples were cut from the top, center and bottom part of the mat and viewed on SEM. Those images were then used to evaluate fiber diameter and alignment.

2.4.3 Image Analysis

Revolution was used to determine the diameter of fibers for JEOL 6400F Field Emission SEM (see Figure 2.5). Three pieces were taken from different parts of each sample, and three SEM images were taken from each piece. Averagely 10 fibers were measured in each SEM images.

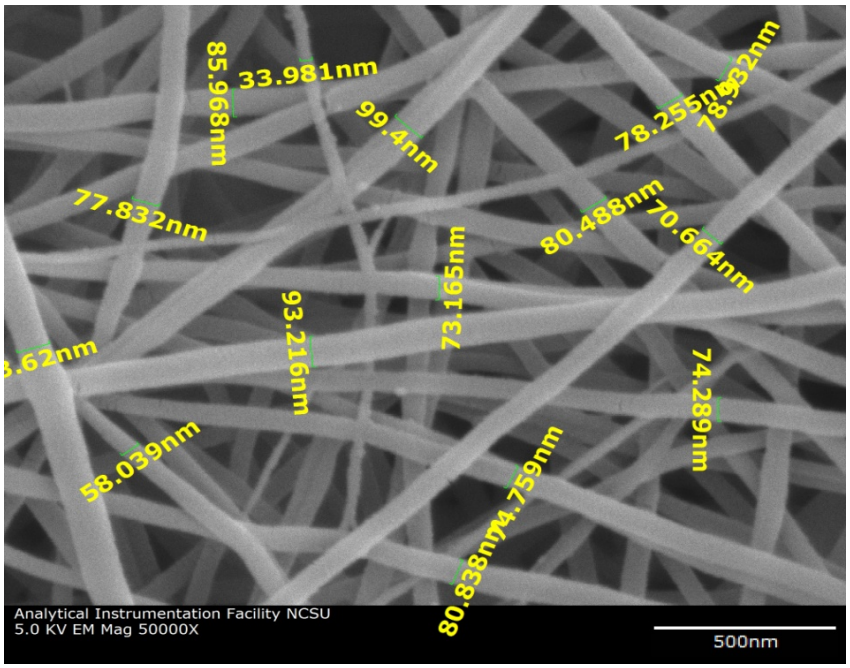

Figure 2.5 Diameter determination from Revolution.

While for images obtained from FEI Phenom, ImageJ was used to measure the diameter of fibers by line length function. Firstly the scaling bar was set according to the scaling bar on the SEM image, and then the line length function gave out the diameter.

ImageJ was also used to measure the void area of the fibrous mats. Firstly the color of fibers and background was changed into black and white by adjusting threshold (see Figure 2.6), then through “analyze particles” function of the software, a report will be created which determins the area fraction of white part, which is the void area fraction. It was calculated as area of single nanofiber layer and used in mechanical property data analysis.

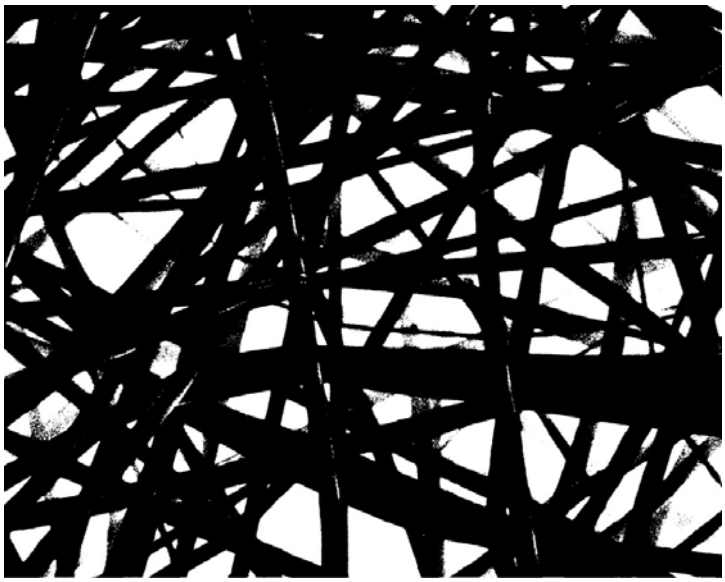

Figure 2.6 Example of thresholded SEM image for void area calculatrion by ImageJ analysis.

2.4.4 Thickness Test

The thickness of fibrous mats was tested on Thwing Albert thickness tester. The tester has a pressure foot and an anvil parallel to the foot. Sample mats were placed on the anvil and the tester provided accurate measurements (±0.001 mm) by utilizing a sensor. Also average, high, low and standard deviation are computed, displayed and can be printed. The average value of sample mats was used in tensile test.

2.4.5 Mechanical Properties Measurement

The tensile behavior of the electrospun nanofibers was tested on an Instron Model 5544 using the Bluehill^{TM} Version 1.00 software with a cross-head speed of 10 mm/min at room temperature. Rectangular tensile specimens were prepared from electrospun nylon 6

nonwoven mats and aligned fiber films. For random fibrous mats, each specimen was cut in to a slide with a planar dimension of width × gauge length = 0.5 inch × 1.125 inch, mounted on a square holder with 1.125 inch gauge length; while for aligned fibrous mats, the specimens were cut into slides with dimension of width × gauge length = 0.5 inch × 0.39 inch. The force vs. extension data was collected using a digital data acquisition hardware and software. Up to eight specimens were tested for each case.

Since void volume is supposed to be proportional to the void area, to eliminate the effect of void volume on mechanical properties, the void area fraction calculated from Image J analyzer was subtracted from total area in that plane.

2.5 Experimental Goals

As mentioned before, the purpose of this investigation is fourfold. First randomly aligned fibers in the form of webs and aligned fibers are to be produced. Secondly we shall investigate the effects of polymer concentration on crystallinity of electrospun nanofibers. Thirdly we will compare the mechanical properties of randomly aligned fibers and aligned fibers. Finally, we will investigate the effect of diameter and fiber orientation on mechanical properties.

CHAPTER 3

RESULTS AND ANALYSIS

3.1 Fiber Morphology

Macroscopically, the electrospun nonwoven nylon 6 mats appear to be a film. Filed emission SEM reveals that, in fact, the electrospun unaligned material is fibrous and highly porous, held together by bonding sites among many fibers. Figure 3.3 shows a series of SEM micrographs illustrating the morphology of the electrospun material and the adhesion/cohesion among the fibers at various bonding sites, which leads to the film-like character and structural integrity of the electrospun fiber mats. The randomly orientated nanofibers are 82±6 to 108 ±11 nm in diameter.

Figure 3.1 is the analysis of electrostatic force on nanofibers when they are collected on two parallel electrodes. F_1 is the electrostatic force resulted from electric field and F_2 is the Coulomb interaction between the positive charges on the fibers and negative charges on the grounded electrodes. These forces were working at two ends of the fiber, and the fiber was stretched and aligned across the gap.

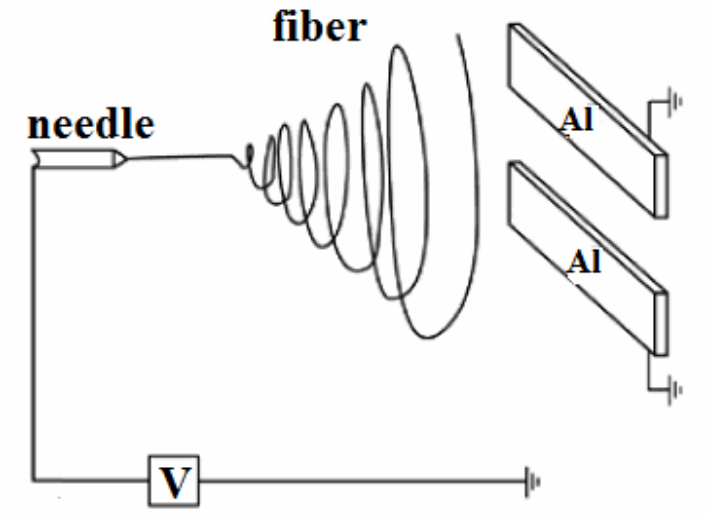

Figure 3.1 Schematic illustration of the setup for generating aligned fibers taken. Figure taken from [30].

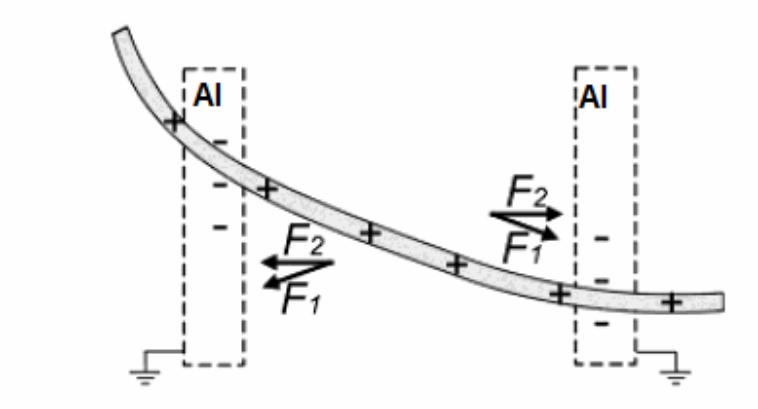

Figure 3.2 Analysis of electrostatic force on nanofibers across the gap. Figure taken from [30].

Figure 3.4 shows the SEM images of electrospun fibers obtained by aligned experiments. The average size of fiber diameter was ranged from 180±12 to 278±16 nm, which is larger than fibers of random electrospun mats (see Figure 3.3). The fibers were spun from the same polymer solution and under the same spinning conditions.

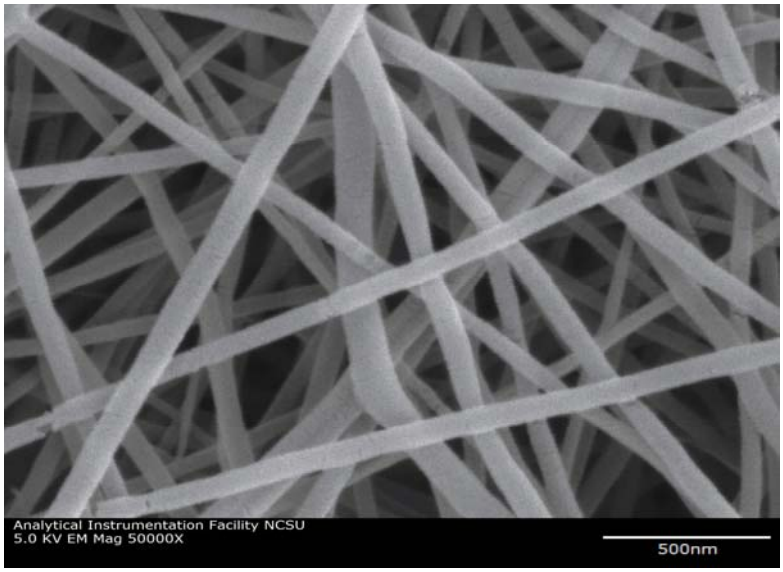

Figure 3.3 Randomly aligned electrospun nylon 6 fibers. The fiber was spun from 15 wt% nylon 6 solution at 15kV, with feed of 10 μL/min and tip-to-collector distance of 15 cm. The average diameter is 82±6 nm.

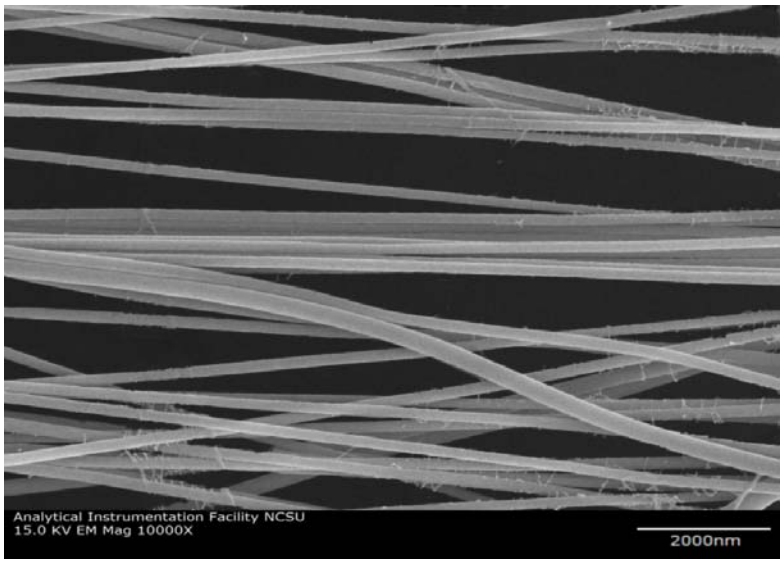

Figure 3.4 Aligned electrospun nylon 6 nanofibers. The fiber was spun from 15 wt% nylon 6 solution at 15kV, with feed of 10 μL/min and tip-to-collector distance of 15 cm. The average diameter is 180±12 nm.

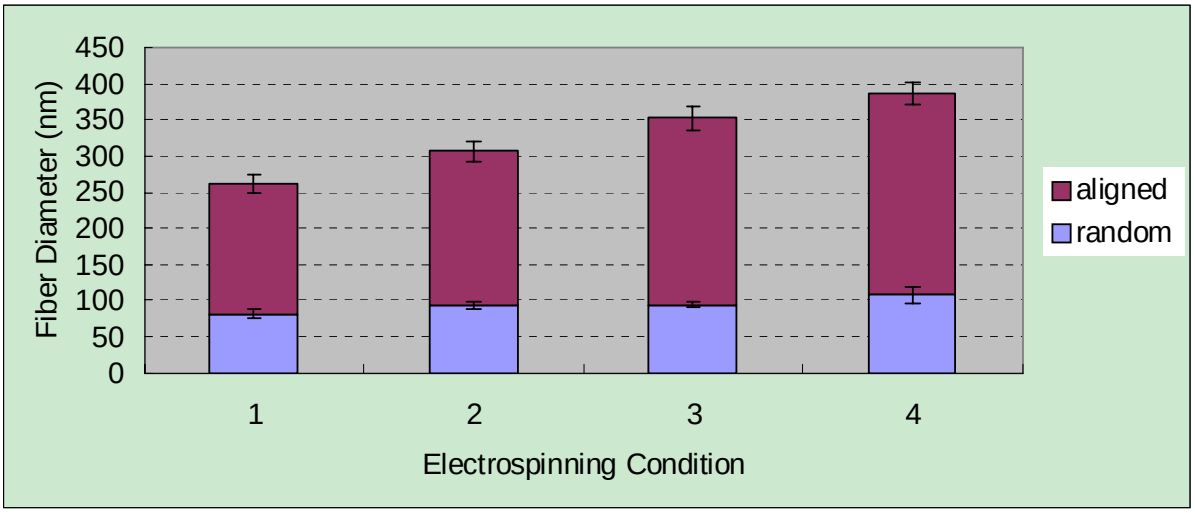

Figure 3.5 Average diameters of random fibers and aligned fibers under the same conditions.

Table 3.1 Spinning conditions and fiber diameters

Condition	Feed Rate (μL/min)	Polymer Concentration (wt%)	Average Diameter of Radndom Fibers (nm)	Average Diameter of Aligned Fibers (nm)	Average Diameter of Random fibers on Parallel Electrodes (nm)
1	10	15	82±6	180±12	87±7
2	10	15	93±5	213±15	92±6
3	15	20	95±4	257±15	98±9
4	15	20	108±11	278±16	114±12

The diameter of unoriented fibers collected on parallel electrodes does not show any difference with random fibers collected by unaligned experiments. The increase of fiber diameter for aligned fibers only occurs in the gap. As Figure 3.7 shows, with the absence of a grounded conductive material between two electrodes, the electric field strength is not as intense as the conductive area. The weaker electric attraction across the gap results in the fibers to relax when spanning across the gap, thus they have larger diameter when aligned between two electrodes.

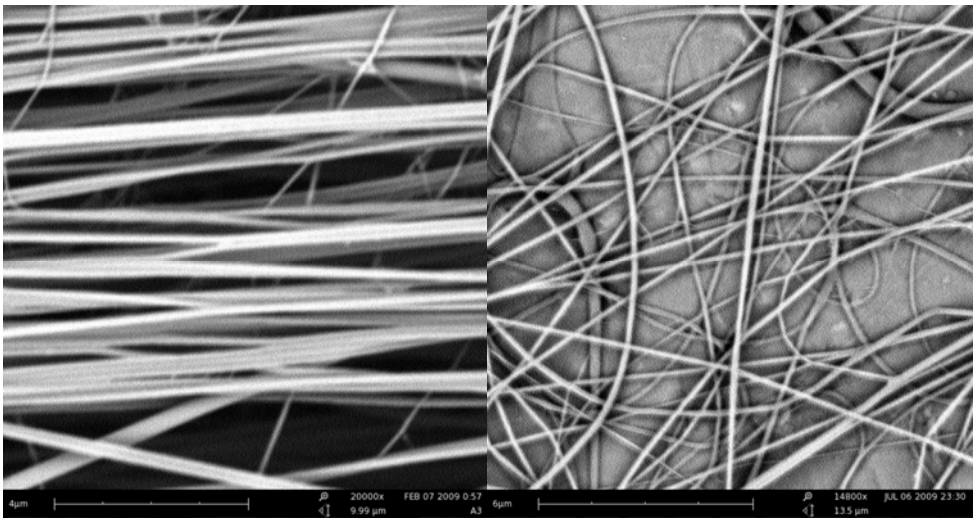

Figure 3.6 SEM images of aligned section and random section at the same magnification for the same sample.

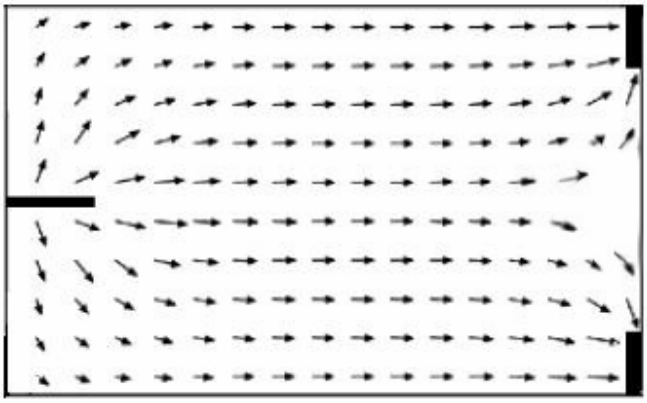

Figure 3.7 Calculated electric field strength vectors in the region between the needle and the collector. The arrows denote the direction of the electrostatic field lines [20].

3.2 Estimation of Crystallinity by DSC

The heat of crystallization (ΔH) of the given sample can be used to estimate the percent of crystallinity of a sample. As all the measurements were done under identical settings of the instrument, the variation of ΔH can be taken to represent the variations of crystallinity in these samples. Table 3.2 gives a summary of ΔH according to the normalized DSC thermograms by sample mass. Generally, ΔH of the electrospun fibers with lower feed rates (10 μL/min) and lower polymer concentrations (15 wt%) are greater than that of fibers with higher feed rates (15 μL/min) and higher concentrations (20 wt%). This indicates the degree of crystallinity of nylon 6 electrospun fibers decreases with the increasing of feed rate and polymer concentration.

Table 3.2 Polymer concentration, feed rate and melting peak area (DSC) of elcctrospun nylon 6 fibers (all the fibers were spun with 15 tip-to-collector distance and 15 kV)

Orientation	Concentration (%)	Feed Rate (μL/min)	ΔH(J/g)	Crystallinity (%)
Aligned	15	10	69.7	36.7
Aligned	20	10	57.6	30.3
Aligned	15	15	64.8	34.1
Aligned	20	15	54.2	28.5
Random	15	10	68.8	36.2
Random	20	10	58.4	30.7

Table 3.2 Continued

Random	15	15	63.6	33.5
Random	20	15	53.9	28.4

For solutions with lower concentrations, there are less polymer chains in the solution, resulting in less chain entanglements, which favors the crystals to be formed. Therefore, for fibers spun from solutions with lower polymer concentration have higher degree of crystallinity.

The increase of crystallinity with the decrease of feed rate can be explained by electrospinning process. When the feed rate is lower, each complete cycle from the tip of needle to grounded collector is relatively longer. Polymers are allowed to whip more completely comparing to higher concentration, thus they are stretched more than polymer with higher feed rate. This causes the crystallinity to increase.

In addition, from Table 3.2, by comparing the crystallinity of rondom fibers and aligned fibers with the same electrospinning conditions, almost the same crystallinity can be found for both forms of fibers. Therefore, the alignment does not change the crystallinity. Crystals probably are formed during the steady jet region and unstable whipping region. The very last microseconds before fibers reach the target has little influence on crystallinity.

3.3 The Effect of Fiber Diameter on Mechanical Properties

The data from uniaxial tensile test show the behavior of the nonwoven electrospun nylon 6 mats is distinctly different from the aligned fiber films. Figure 3.8 and Figure 3.9 are plots comparing the Young's modulus and tensile strength of electrospun nylon 6 non-woven and aligned electrospun nylon 6 fibers. In general, the aligned fibers have much higher modulus and tensile strength than unoriented fibers.

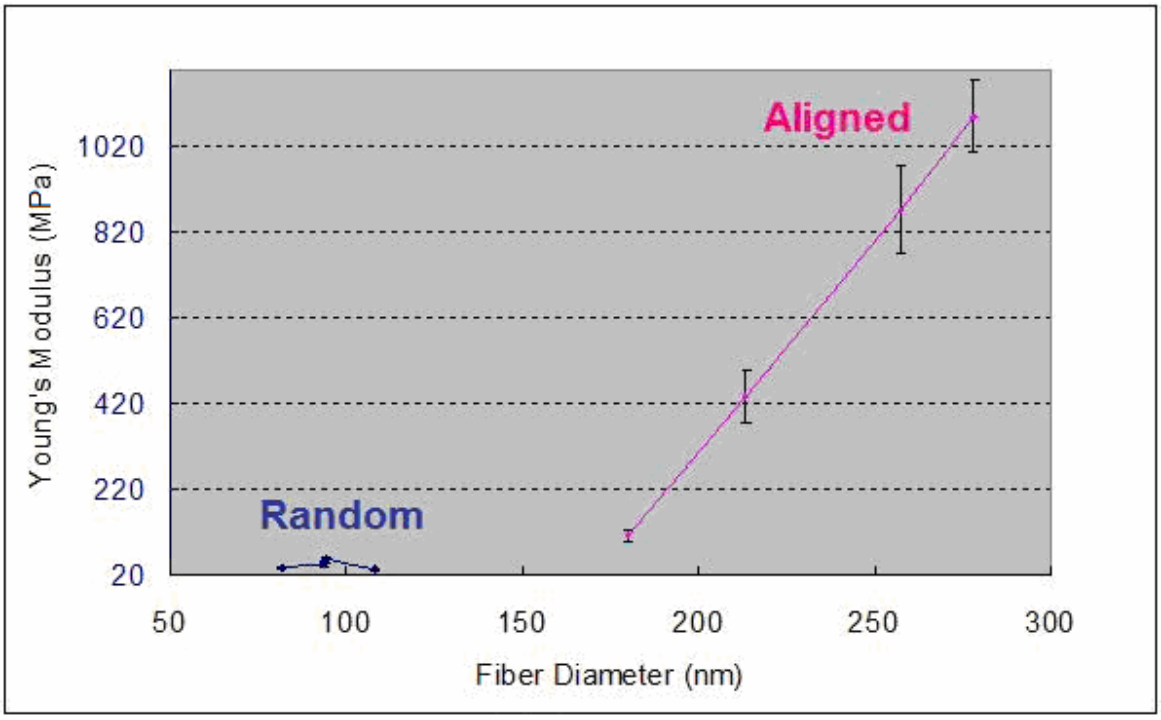

Figure 3.8 Young's modulus vs. fiber diameter curves for randomly aligned fiber mats (blue) and aligned fiber film (pink)

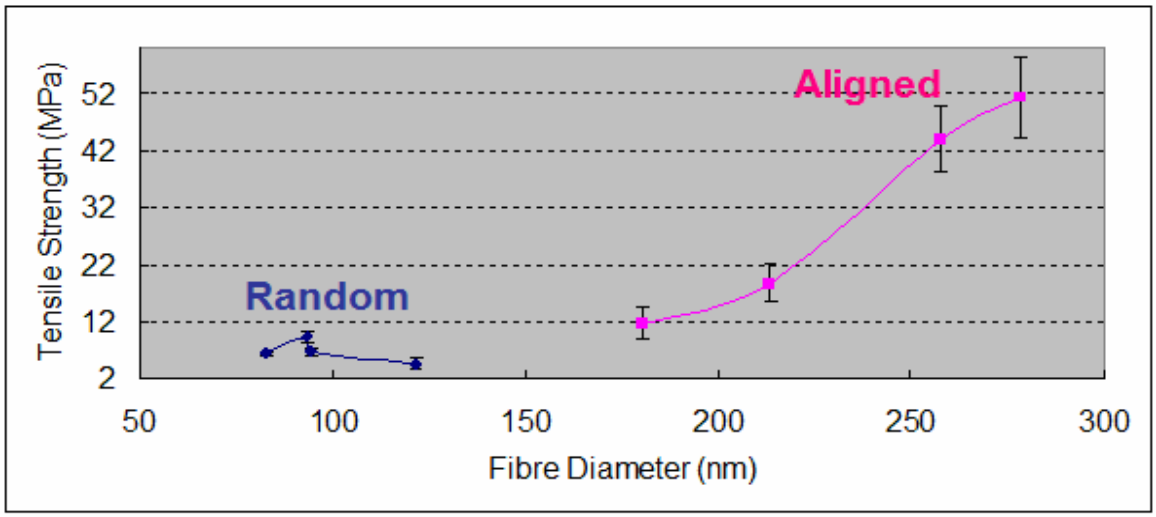

Figure 3.9 Tensile strength vs. fiber diameter curves for randomly aligned fiber mats (blue) and aligned fiber film (pink)

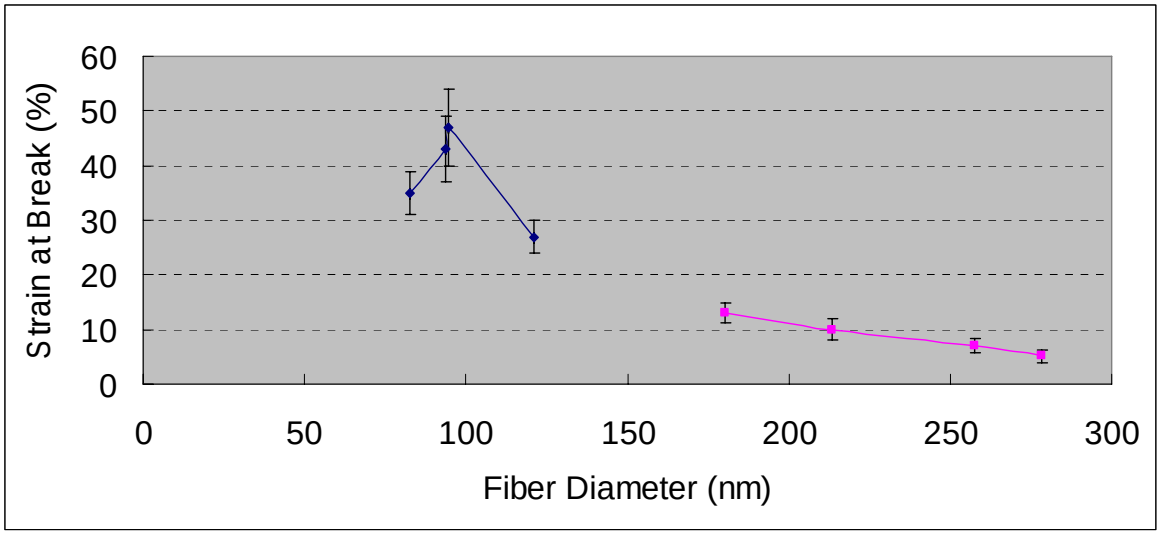

Figure 3.10 Strain at break vs. fiber diameter curves for randomly aligned fiber mats (blue) and aligned fiber film (pink)

The difference between mechanical properties of random fibers and aligned fibers probably is caused by different breaking mechanisms. When a strain is applied to the electrospun mat, fibers oriented in the direction of cross-head displacement are stretched uniaxially, while fibers oriented at some angle relative the principal strain direction experience a rotation. Eventually, the junctions and adhesion between fibers at various bonding sites are broken before the fibers are broken. However, for aligned fiber films, the fibers have already been oriented at the direction of displacement. The strain is loaded along fibers themselves, and most fibers are stretched until they are broken. In addition, there is much less fiber rotation compared to nonwoven fiber mats. This explains lower Young's modulus and tensile strength, but higher strain at break in unaligned nonwoven mats. The fundamental difference observed in the tensile behavior of the two forms of nanofibers may be deciphered by morphological characterization of broken fibers.

Figure 3.11 is SEM images of broken edge of nonwoven electrospun mats and aligned fiber film. In these images, random webs of nanofibers appear to fail at the junctions between fibers and not by fiber breakage, and the fiber threads can be observed at the broken edge. In contrast, aligned nanofiber webs appear to fail due to breakage of the fibers. This confirms different mechanisms of break for the randomly aligned nanofiber mats and aligned nanofiber films.

These mechanisms also explain the effect of fiber diameter on mechanical properties of nonwoven electrospun mats and aligned nanofiber films. Since nonwoven mats are broken due to the failure of cohesions among fibers, the mechanical properties are independent of fiber properties (such diameter and crystallnity of fibers). While aligned fibrous mats fail because of the breakage of fibers themselves, the individual fibers comprising the mat are responsible for the mechanical properties of the whole mat.

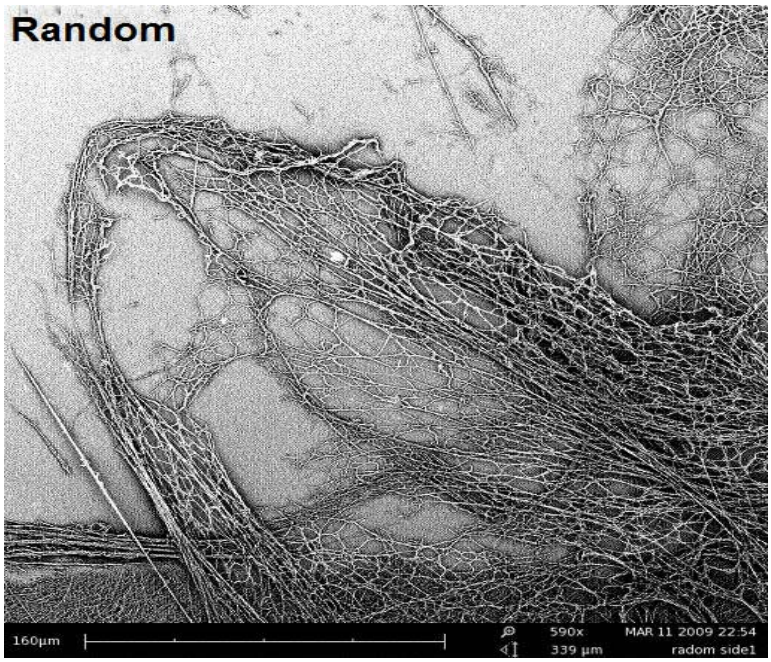

(a)

Figure 3.11 SEM images of broken edge of random fibers((a),(b)) and aligned fibers ((c))

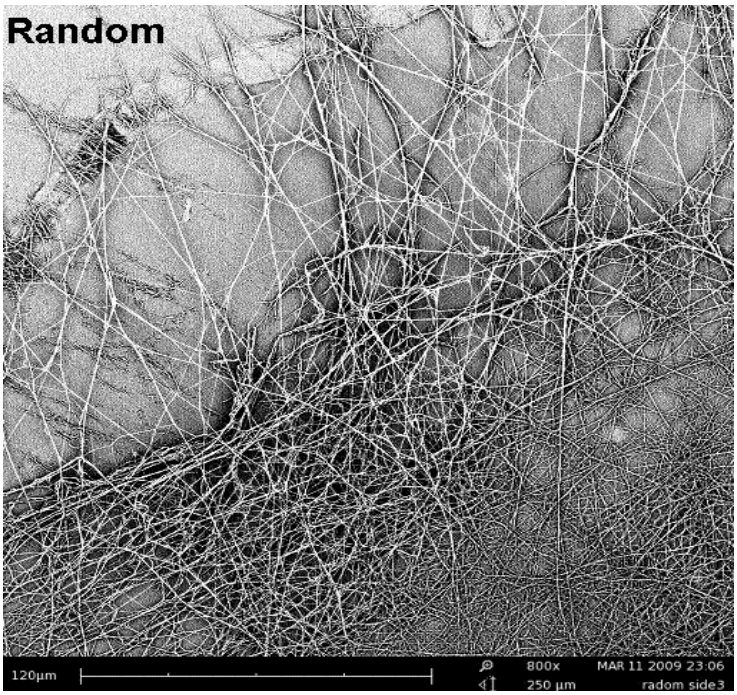

(b)

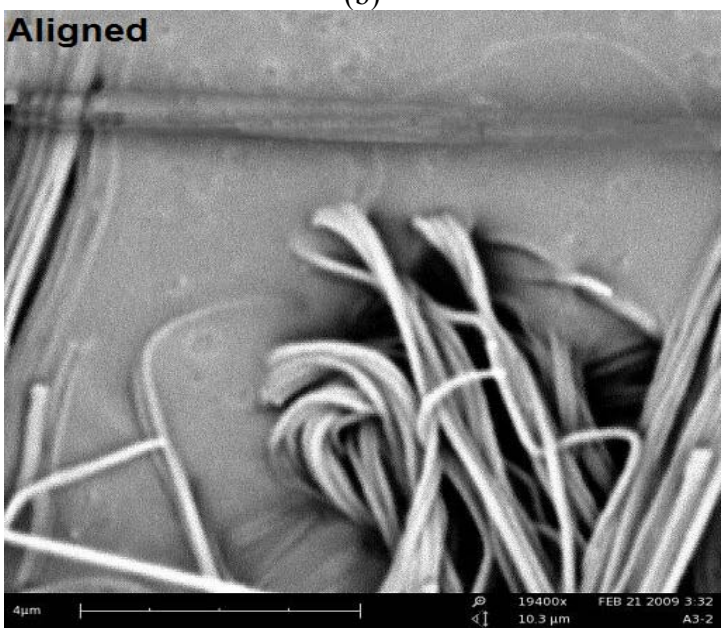

(c)

Figure 3.11 Continued SEM images of broken edge of random fibers((a),(b)) and aligned fibers ((c))

For aligned fibrous mats, according to the standard formula calculating Yong's modulus, since the modulus was normalized by cross-sectional area of fibrous mats, it should be independent on fiber diameter under the same strain and gauge length.

$$\mathrm{E} = \frac{\sigma}{\varepsilon} = \frac{FL_0}{A_0 \Delta L} \qquad Equation\ 7$$

However, the data in our study shows a dependence on diameter (see Figure 3.5). This is mainly due to two reasons. Firstly, it requires higher number of fibers with smaller diameter to reach the same cross-sectional area than larger fibers. This could result in a higher chance for each individual fiber having defects. Those fibers with defects are easier to break, and they are lost during the tensile test. Therefore, the Yong's modulus is lower for fibers with smaller diameter. Furthermore, even for aligned fibers, the alignment is not perfect. Not all the fibers are aligned with the direction of strain. The higher number of smaller fibers would increase the chance of imperfect alignment, which results in the decrease of modulus.

Figure 3.12 reveals the relationship between the crystallinity of material and its Young's modulus. If the electrospun fibers possess higher degree of crystallinity, which means better molecular orientation, this crytallinity/orientation will partially account for the smaller diameter of fibers in the aligned electrospun nylon 6 mats (see Table 3.3). As mentioned before, with larger diameter, the fibers are less likely to have defects, and the breakage is more likely to start at a cross-sectional area rather than from weak points, which is a

contributing factor to the “stiffer” response of the aligned electrospun nanofibers when tested in uniaxial tension.

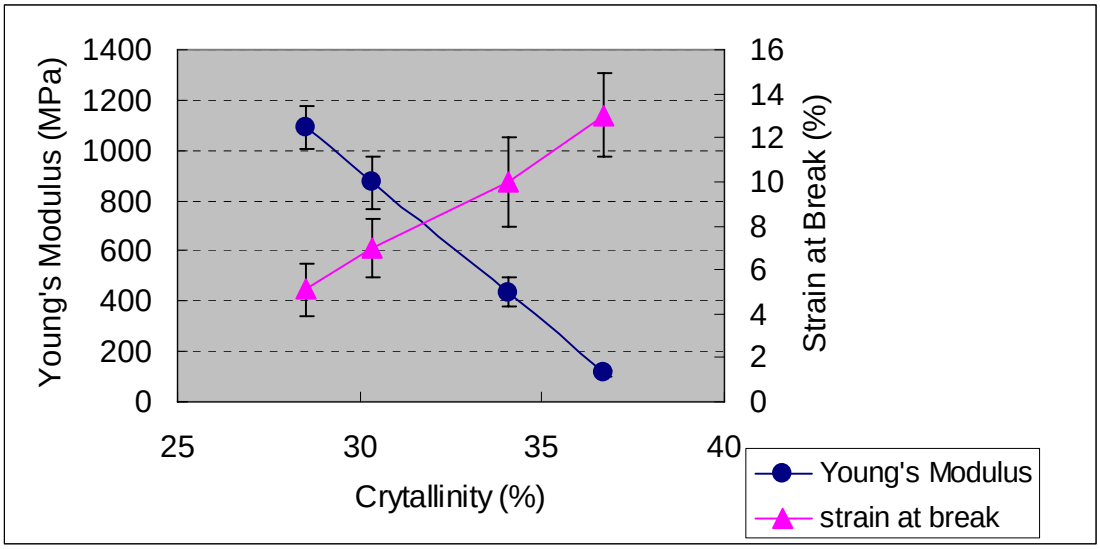

Figure 3.12 Young’s Modulus and strain at break of aligned fibers at different crystallinity

Table 3.3 The crystallinity and fiber diameter of aligned fibers

Average Diameter (nm)	Crystallinity (%)
180±12	36.7
213±15	33.5
257±15	30.7
278±16	28.5

However, in the other hand, the change in percent of crystallinity is small (from 28.5% to 36.7%). Maybe it is not big enough to make a difference in the mechanical properties.

The crystallinity and its effect on mechanical properties of random fibrous mats, it suggests mechanism of break of nonwoven electrospun fibrous mats is different than the aligned fibrous mats. Figure 3.13 shows the independence of fiber crystallinity on Young's modulus for unaligned fibrous mats. Since individual fibers are not responsible for the mechanical behavior of the whole mat, there is no necessary relationship between crystallinity and mechanical properties. However, the percent of crystallinity does not tell us about the orientation of the polymers or crystals. In this study, we assume that they align in the fiber direction. Further study need to be conducted by X-ray diffraction which will be discussed in chapter 4.

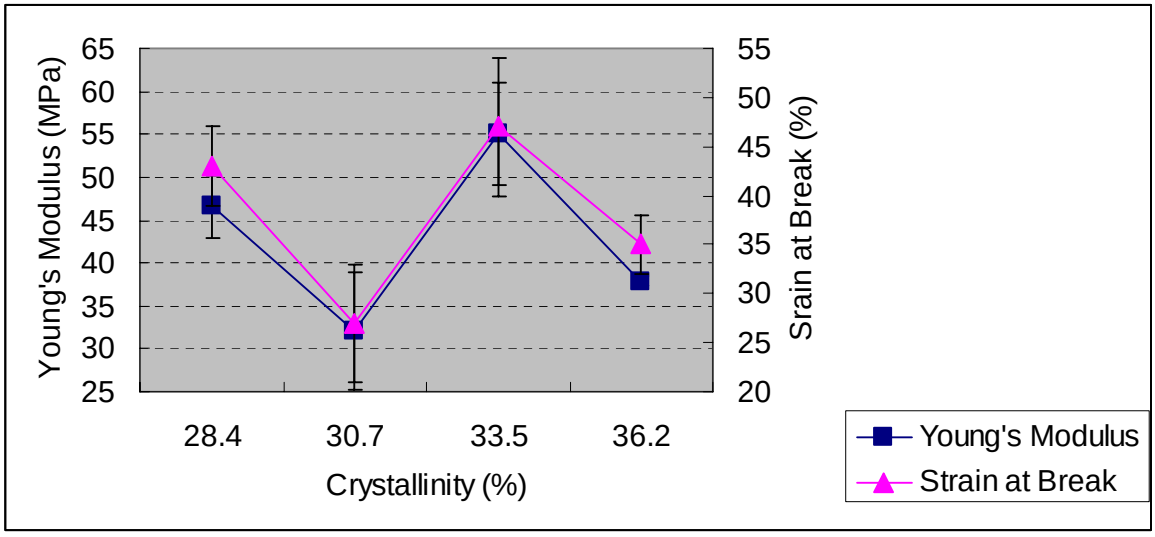

Figure 3.13 Young's modulus and strain at break at different crystallinity of unaligned fibers

CHAPTER 4

CONCLUSIONS AND FUTURE WORK

Two forms of electrospun fibers were produced by normal and aligned electrospinning methods. The randomly aligned fiber mats were collected on a large, flat, grounded target, while the aligned fibers were created by parallel collecting electrodes. Electron microscopy was used to illustrate the morphology of the electrospun fibers. The results showed that higher concentration could produce larger fibers due to more polymer chains and chain entanglements.

DSC was also employed in this study to investigate the effect of polymer concentration on crystallization of nylon 6. The data revealed that the crystallinity of fibers increases as the concentration and feed rate decrease. This is because with lower concentration, there are less entanglements and less fibers within the same amount solution, the fibers are easier to be stretched and oriented which favors the crystals to be formed. Also, with lower feed rate, fibers are allowed to whip more completely comparing to higher feed rate, therefore, fibers are more likely to spread out which resulting in the increase of crystallinity.

By analyzing SEM images of electrospun fibers, the aligned fibers are larger than the unaligned fibers collected on the parallel electrodes and those produced by unaligned experiments. This is because of reduction of the electric field in the gap area. Comparing to the whole piece of conductive grounded collector, the electrical attraction between two

parallel electrodes is weaker and causes the fibers to relax when spanning across the gap. Therefore, the aligned fibers have larger diameter.

The mechanical behavior of these two fibers has been observed and compared to each other. The aligned fibrous mats processed much higher Young's modulus and tensile strength than unaligned fibrous mats. This is due to that these two forms of electrospun nanofibers have characteristically different responses to strain resulting from two breaking mechanisms: the nonwoven mats were broken due to the failure of junctions and cohesion among the fibers at the bonding sites; however, the aligned nanofibers comprising the mat were oriented in the direction of stretching, thus mats were broken when the individual fibers were broken. The mechanisms were confirmed by SEM images of broken edges of these two forms of fibers. Through the images, the delamination phenomenon was observed on nonwoven nanofiber mats. However, for aligned nanofiber films, the individual fibers were completely broken. The mechanical data also revealed that for aligned fibers as fiber diameter increases, the Young's modulus also increases. While theoretically Yong's modulus should be independent on fiber diameter. There are two reasons: firstly, to have the same cross-sectional area, the higher number of smaller fibers is required and this would increase the chance of fiber having defects which cause the fibers easier to be broken. Secondly, the alignment is not perfect. Higher number of smaller fibers has more chances to be unoriented with the direction of strain, thus they have lower Yong's modulus compared to larger fibers. In addition, by correlating the crystallinity obtained from DSC and fiber mechanical properties,

it indicated higher degree of crystallinity leads to lower Young's modulus for the aligned nanofibers. Because higher crystallinity means polymer chains are more oriented which results in smaller diameter, as discussed above, with smaller diameter, fibers have more chance to have defects, which makes them easier to break and the modulus was lost during crosshead displacement and results in lower modulus.

Proposal experiments:

This study provides a basic understanding of the relationship between mechanical properties and structures, fiber orientation of electrospun fibers, but further investigation is required to pinpoint relationships, reduce error, and establish a broader range of data.

1. Dynamic mechanical analysis (DMA)

This experiment could measure the dynamic response of the nylon 6 under different conditions. The analysis of the storage modulus and loss tangent curves is very useful in ascertaining the performance of electrospun nanofibers under stress and temperature.

2. WAXD

WAXD curves could determine the structural parameters of crystal in the fibers. From the results of WAXD, the effect of operating parameters during electrospinning on microscopic structure of fibers can be studied. Furthermore, through WAXD curves, the orientation degree of crystals can be determined by Hermans orientation function. This function will

quantify the fiber alignment. In this study, we assume the crystals in the fibers align in the fiber direction which and use the percent of crystallinity to represent the fiber orientation, but with WAXD the evaluation of the contribution of fiber orientation to mechanical properties of electrospun nanofibers could be more accurate.

3. Infrared dichoroism (IR)

Molecular orientation in the electrospun fibers can be shown with polarized infrared spectroscopy. This will help isolate the effect of molecular orientation in the electrospun fibers. An orientation function can also be calculated using the dichroic ratios from IR absorption. Dichroic ratios could be computed using peak values obtained from IR spectra of oriented electrospun samples with linearly polarized light parallel and perpendicular to the principle direction of fiber orientation.

By conducting these experiments, the mechanical behavior of electrospun nanofibers can be understood by combining macro, micro, and molecular scale characterization.

REFERENCES

1. Morton W. J.. Methods of Dispersing Fluids. *US Patent*, 705,691.
2. Formhals A.. Processing and Apparatus for preparing artificial threads. *US Patent* 2,077,373, 1934.
3. Formhals A.. Method of producing artificial fibers. *US Patent* 2,158,415, 1939.
4. Formhals A.. Production of artificial fibers from fiber forming liquids. U*S Patent* 2,323,025, 1943.
5. Formhals A.. Method and apparatus for spinning. *US Patent* 2,349,950, 1944.
6. Zeleny J.. The electrical discharge from liquid points, and a hydrostatic method of measuring electric intensity at their surfaces. *Physical Reviews*. 1914;**3:** 69-91.
7. Baumgarten P.. Electrostatic spinning of acrylic microfibers. *Journal of Colloid and Interface Science*. 1971;**36:** 71-79.
8. Larrondo L., Manley R. S.. Electrostatics fiber spinning from polymer melts. *Polymer Science: Part B: Polymer Physics.* 1981;**19:** 909-920.
9. Doshi J., Reneker D. H.. Electrospinning process and applications of elecrospun fibers. *Journal of Electrostatics.* 1995;**35:** 151-160.
10. Theron A., Zussman E, Yarin A.L.. Electrostatic field-assisted alignment of electrospun nanofiber. *Nanotechnology.* 2001;**12:** 384-390.
11. Deitzel J. M., Kleinmeyer J. D., Hirvonen J. K., Tan N. B.. Controlled deposition of electrospun poly(ethylene oxide) fibers. *Polymer.* 2001;**42:**8163-8170.
12. Reneker D. H., Chun I.. Nanometer diameter fibers of polymer, produced by

electrospinning. *Nanotechnology,* 1996;**7:**216-223.

13. Ganan-Calvo A. M., Barrero A.. Current and droplet size in the electrospraying of liquid scaling laws. *Journal of Aerosol Science*, 1997;**28**(2): 249-275.
14. Hartman R. P. A., Camelot D. M. A., Marijnissen J. C. M.. Electrohydrodynamic atomization in the cone-jet mode: Physical modeling of the liquid cone and jet. *Journal of Aerosol Science,* 1999. **30**(7): 823-849.
15. Taylor S. G.. The force exerted by an electric field on a long cylindrical conductor. *Proceedings of the royal society of London.* 1965;**Series A:** 145-158.
16. Taylor S. G.. Electrically driven jets. *Proceedings of the Royal Society of London Series A, Mathematical and Physical Science.* 1969;**313:** 453-475.
17. Cloupeau M., Prunet-Foch B.. Electrohydrodynamic spraying functioning modes- A critical review. *Journal of Aerosol Science.* 1994;**25:** 1021.
18. Ganan-Calvo A.. Cone-Jet analytical extension of Taylor's electrostatic solution and the asymptotic universal scaling law in electrospraying. *Physical Review Letters.* 1997;**79:** 217.
19. Hohman M. M., Shin M., Rutledge G., Brenner M. P.. Electrospinning and electrically forced jets. I. Stability theory. *Physics of Fluids.* 2001;**13:** 2201-2220.
20. Feng J. J.. The stretching of an electrified non-Newtonian jet: A model for electrospinning. *Physics of Fluids.* 2002;**14:** 3912-3926.
21. Carroll C. P., Joo Y. L.. Electrospinning of viscoelastic Boger fluids: Modeling and experiments. *Physics of Fluids.* 2006;**18:** 14.

22. Sergey V., Fridrikh, J. H. Y., Michael P., Gregory C.. Controlling the fiber diameter during electrospinning. *Physical Review Letters,* 2003;**90**(14).

23. Deitzel J. M., Harris D., Beck Tan N. C.. The effect of processing variables on the morphology of electrospun nanofibers and textiles. *Polymer,* 2001. **42**(2001): 261-272.

24. Fong H., Reneker D. H.. Beaded nanofibers formed during electrospinning. *Polymer,* 1999. **40:** 4585-4592.

25. Shin Y. M., Brenner M. P., Rutledge G. C., Electrospinning: A whipping fluid jet generates submicron polymer fibers. *Applied Physics Letters,* 2001;**78**(8):1149-1151.

26. Shin Y. M., Brenner M. P., Rutledge G. C., Experimental characterization of electrospinning: the electrically forced jet and instabilities. *Polymer,* 2001;**42:** 9955-9967.

27. Moses H., Gregory R., Michael P.. Electrospinning and electrically forced jets. II. Applications. *Physics of Fluids,* 2001;**13**(8).

28. Moses H., Gregory R., Michael P.. Electropinning and electrically forced jets. I. Stability theory. *Physics of Fluids,* 2001;**13**(8).

29. Murty, N. K.. The stability of a dielectric liquid jet in the presence of a longitudinal electric field. *Proceeding of the Physical Society,* 1960. **75**: 369-373.

30. Dan L., Yun X.. Fabrication of titania nanofibers by electrospinning. *Nano Letters,* 2003;**3**(4): 555-560.

31. Zheng M. H., Ying Z. Z., Kotaki M., Ramakrishna, S.. A review on polymer nanofibers by electrospinning and their applications in nanocomposites. *Composites Science and Technology,* 2003;**63:** 2223-2253.

32. Timothy G.. Polymeric nanofibers and nanofiber webs: A new class of nonwovens. *Proceeds of INTC 2002: International Nonwovens Technical Conference.* 2002. Atlanta, Georgia: Donaldson Company Inc.

33. Dan L., Yun X., Yuliang W.. Electrospinning of polymeric and ceramic nanofibers as uniaxially aligned arrays. *Nano Letter.,* 2003;**3**(8): 1167-1171.

34. Flemming R. G., Murphy C. J., Abrams G. A., Goodman S. L., Nealey P. F.. Effects of synthetic micro-and nano-structured surfaces on cell behavior. *Biomaterials.* 1999;**20:** 573-588.

35. Mathew J. A. Wnek G. E., Simpson D. G., Bowlin G. L.. Electrospinning of collagen nanofibers. *Biomacromolecules.* 2002;**3:** 232-238.

36. Li W. J., Laurencin C., Caterson E., Tuan R., Ko F.. Electrospun nanofibrous structure: A novel scaffold for tissue engineering. *Journal of Biomedical Materials Research.* 2001; **60:** 612.

37. Katta P., Alessandro M., Ramsier R. D., Chase G. G.. *Nano Lett.* **2004**, *4*, 2215.

38. Yi X., Zhonghao H., Jinfeng C., Cheng W., Yanbin T., Sidong L.. *Materials Letters* 2008, **62**:991-993.

39. Dersch, R., Liu T., Schaper, A. K., Greiner, A., Wendorff, J. H.. *J. Polym. Sci. Part B* 2003, **41**:545.

40. Surawut Chuangchote, Pitt Supaphol. *J. of Nanosci. and Nonotech.* **2006**, **6**:125-129.

41. Ying Y., Zhidong J., Qiang L, Liming W., Zhicheng G.. *International Conference on Solid Dielectrics, Winchester, UK,* 2007.

42. Soumayajit S., Seetharama D., Gary T.. *Macromolecular* 2007, **28**:1034-1039.

43. Dayong Y., Bo L., Yong Z., Xingyu J.. *Advanced Materials* 2007, **19**:3702-2706.

44. Jin H. J., Chen J. S., Karageortgious V., Altman G. H., Kaplan D. L.. Human bone marrow stromal cell response on electrospun silk fibroin mats. *Biomaterials.* 2004,**25**: 1039-1047.

45. Min B. M., You Y, Kim J. M., Lee S. J., Park W. H. Formation of nanostructured poly(lactic-co-glycolic acid)/chitin matrix and its cellular response to normal human keratinocytes and fibroblasts. *Carbohydrate Polymers.* 2004;**57**: 285-292.

46. Xu C.Y. Inai R, Kotaki M, Ramakrishna S. Aligned biodegradable nanotibrous structure: a potential scaffold for blood vessel engineering. *Biomaterials.* 2004;**25**: 877-886.

47. Shin M., Ishii O., Sueda T., Vacanti J. P. Contractile cardiac grafts using a novel nanofibrous mesh. *Biomaterials.* 2004;**25**: 3717-3723.

48. Riboldi S. A., Sampaolesi M., Neuenschwander P., Cossu G., Mantero S.. Electrospun degradable polyesterurethane membranes: potential scaffolds for skeletal muscle tissue engineering. *Biomaterails.* 2005;**26**: 4606-4615.

49. Li W. J., Tuli R., Huang X. X., Laquerriere P., Tuan R. S.. Multilineage differentiation of human mesenchymal stem cells in a three-dimensional nanofibrous scaffold. *Biomaterials.* 2005;**26:** 5158-5166.

50. Telemeco T. A., Ayres C., Bowlin G. L.. Regulation of cellular infiltration into tissue engineering scaffolds composed of submicron diameter fibrils produced by electrospinning. *Acta Biomater.* 2005;**1**: 377-385.

51. Caruso R. A., Schattka J. H., Greiner A.. Titanium dioxide tubes from sol-gel coating of electrospun polymer fibers. *Advanced Materials.* 2001;**13**: 1577.

52. Kataphinan W., Reneker D. H., Teye-Mensah R., Evans E. A., Ramiser R., Smith D. J.. Electrospinning titanium alkoxide precursor with rare earth compounds. Abstracts of Papers of the American Chemical Society. 2003;**226**: U402-U402.

53. Drew C., Liu X, Ziegler D., et al. Metal oxide-coated polymer nanofiber. *Nano Letters.* 2003;**3**: 143-147.

54. Shao C., Kim H., Gong J., Lee D. A novel method for making silica nanofibers by using electrospun fiber of polyvinylacohol/silica composite as precursor. *Nanotechnology.* 2002;**13**: 635-637.

55. Guan H. Y., Shao C. L., Chen B., Gong J., Yang X. H.. A novel method for making CuO superfine fibers via an electrospinning technique. *Inorganic Chemistry Communications.* 2003;**6:** 1409-1411.

56. Wang Y., Serrano S., Santiago-Aviles J. J.. Conductivity measurement of electrospun PAN-based carbon nanofiber. *Journal of Materials Science Letter.* 2002;**21**: 1055-1057.

57. Gu S. Y., Ren J., Wu Q. L.. Preparation and structures of electrospun PAN nanofibers as a precursor of carbon nanofibers. *Synth Met.* 2005; **155**: 157-161.

58. Hou H. Q., Ge J. J., Zeng J.. Electrospun polyacrylonitrile nanofibers containing a high contraction of well-aligned multiwall carbon nanotubes. *Chemistry of Materials.* 2005;**17**: 967-973.

59. Ma M.L., Mao Y., Gupta M., Gleason K.K., Rutledge G.C. Superhydrophobic fabrics

produced by electrospinning and chemical vapor deposition. *Macromolecules.* 2005;**38**: 9742-9748.

60. Wang Y., Serrano S., Santiago-Aviles J. J.. Conductivity measurement of electrospun PAN-based carbon nanofiber. *Journal of Materials Science Letters.* 2002;**21**: 1055-1057.
61. Kenawy E. R., Bowlin G. L., Mansfield K.. Release of tetracycline hydrochloride from electrospun polymers. *Abstracts of Papers of the American Chemical Society.* 2002;**223**: C115-C115.
62. Satyajeet O., Mehdi A., Richard K., Russell G.. Morphology of electrospun nylon-6 nanofibers as a function of molecular weight and processing parameters. *Journal of applied polymer science.* 2008;**108**: 308-319.

APPENDICES

For additional information, the data used in this thesis is listed as Table A.1 and Table A.2. Table A.1 is the cytstallinity and fiber diameter of fibers electrospun under different conditions. Table A.2 is the mechanical data obtained from tensile tests on Instron.

Table A.1 Electrospinning conditions, produced fiber diameter and fiber crystallinity (all the fibers are spun with 15 cm tip-to-collector distance and 15kV)

Alignment	**Feed Rate (μL/min)**	**Concentration (wt%)**	**Average Diameter (nm)**	**Crystallinity (%)**
Random1	10	15	81±5	36.2
Random2	10	20	94±4	30.7
Random3	15	15	93±5	33.5
Random4	15	20	108±11	28.4
Aligned1	10	15	180±12	36.7
Aligned2	10	20	257±15	30.7
Aligned3	15	15	213±15	33.5
Aligned4	15	20	278±16	28.4
Random*1	10	15	87±7	N/A
Random*2	10	20	92±6	N/A
Random*3	15	15	98±9	N/A
Random*4	15	20	114±12	N/A

(Random* means random fibers collected on parallel electrodes)

Table A.2 Mechanical property data

Alignment	Tensile Strength (MPa)	Standard Error of Tensile Strength	Young's Modulus (MPa)	Standard Error of Young's Modulus	Strain at break (%)	Standard Error of Strain
Random1	6.414	0.345	37.913	3.68	35	4.1
Random2	9.362	1.008	46.613	6.82	43	6.3
Random3	6.832	0.51	55.100	5.97	47	7.2
Random4	4.52	0.92	32.149	0.61	27	3.4
Aligned1	11.7	2.67	114.030	12.9	13	1.9
Aligned2	18.76	3.46	436.300	60.12	10	2.1
Aligned3	44.123	5.77	871.164	101.77	7	1.3
Aligned4	51.33	6.95	1090.012	83.63	5	1.2

The Effect of Polymer Concentration on Fiber Morphology

In this study, we also investigated into the effect of polymer concentration on fiber diameters. Polymer solutions are essentially non-Newtonian fluid; elongation flow resists the break up of the viscoelastic jet, leading to the formation of long threads of mini jets. As a result, the morphology of the nanofibrous structure depends on the factors that affect viscosity (such as concentration)[62]. Figure A.1 shows the diameter distribution for nylon 6 samples at different concentrations (at 15 kV, 15 cm, and 15 μl/ min). By increasing the concentration

and feed rate, the fiber diameters grow and the distribution become wider. Diameters of fibers produced mainly distributed between 60-90 nm at 10 wt %, 70-100 nm at 12 wt % and 110-150 at 15 wt %. This is due to more chain entanglement which decreases the mobility of polymer chains. Therefore, at higher concentration less extension is expected and overall fiber diameter increases.

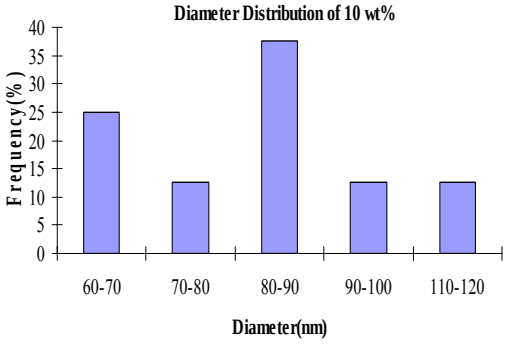

(a)

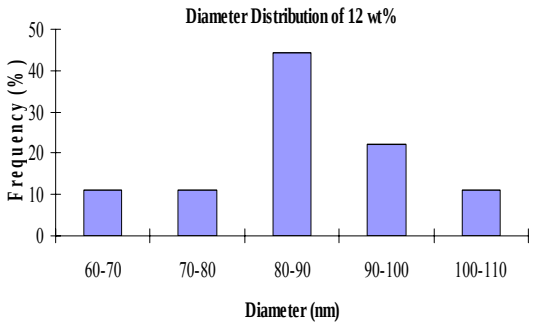

(b)

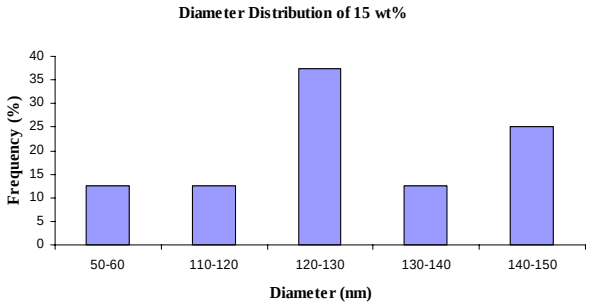

(c)

Figure A.1 Fiber diameter distribution of various concentrations ((a)-(c))